Manuscript prepared for Geosci. Model Dev. Discuss.
with version 2014/05/30 6.91 Copernicus papers of the LaTeX class copernicus.cls.
Date: 9 December 2015

First implementation of Secondary Inorganic Aerosols into the chemistry transport model MOCAGE version R2.15.0

J. Guth[1], **B. Josse**[1], **V. Marécal**[1], **M. Joly**[1], **and P. hamer**[2,1]

[1]Centre National de Recherches Météorologiques/Groupe d'étude de l'Atmosphère Météorologique, CNRS–Météo-France, UMR3589, Toulouse, France
[2]NILU – Norwegian Institute for Air Research, PO box 100 NO-2027, Kjeller, Norway

Correspondence to: J. Guth (jonathan.guth@meteo.fr)

Abstract

In this study we develop a Secondary Inorganic Aerosol (SIA) module for the chemistry transport model MOCAGE developed at CNRM. The aim is to have a module suitable for running at different model resolutions and for operational applications with reasonable computing times. Based on the thermodynamic equilibrium module ISORROPIA II, the new version of the model is presented and evaluated both at the global and regional scales.

The results show high concentrations of secondary inorganic aerosols in the most polluted regions: Europe, Asia and the eastern part of North America. Asia shows higher sulfate concentrations than other regions thanks to emission reductions in Europe and North America.

Using two simulations, one with and the other without secondary inorganic aerosol formation, the global model outputs are compared to previous studies, to MODIS AOD retrievals, and also to in situ measurements from the HTAP database. The model shows a better agreement with MODIS AOD retrievals in all geographical regions after introducing the new SIA scheme. It also provides a good statistical agreement with in situ measurements of secondary inorganic aerosol composition: sulfate, nitrate and ammonium. In addition, the simulation with SIA generally gives a better agreement with observations for secondary inorganic aerosol precursors (nitric acid, sulfur dioxide, ammonia) in particular with a reduction of the Modified Normalised Mean Bias (MNMB).

At the regional scale, over Europe, the model simulation with SIA is compared to the in situ measurements from the EMEP database and shows a good agreement with secondary inorganic aerosol composition. The results at the regional scale are consistent with those obtained from the global simulations. The AIRBASE database was used to compare the model to regulated air quality pollutants: particulate matter, ozone and nitrogen dioxide concentrations. Introduction of the SIA in MOCAGE provides a reduction in the $\mathrm{PM}_{2.5}$ MNMB of 0.44 on a yearly basis and up to 0.52 for the three spring months (March, April, May) when SIA are at their maximum.

1 Introduction

Aerosols are a suspension of airborne solid or liquid particles, with a typical size between a few nanometres and $10\,\mu\mathrm{m}$, that reside in the atmosphere from at least several hours (Stocker et al., 2013) and up to several days. Atmospheric aerosols play a key role in various fields. Their radiative properties allow them to absorb and scatter radiation and play a significant role in the global climate system especially in a climate change context. The estimation of radiative forcing due to aerosols is negative, but with a strong uncertainty. Most aerosols seem to have a cooling effect except for black carbon (Stocker et al., 2013). This radiative aspect also affects the horizontal dimension while being a possible source of visibility reduction (Bäumer et al., 2008).

Aerosols are also important pollutants affecting air quality. Aerosols in air quality applications are characterised in terms of Particulate Matter (PM). PM_x is the amount of particulate matter with diameters less than x microns. PM_{10} and $\mathrm{PM}_{2.5}$ are measured quantities and used for the legal concentrations in air quality regulations. The World Health Organization's guidelines for particulate matter are a $20\,\mu\mathrm{g\,m}^{-3}$ annual mean for PM_{10} and a $10\,\mu\mathrm{g\,m}^{-3}$ annual mean for $\mathrm{PM}_{2.5}$ (WHO, 2006).

One can distinguish between primary aerosols, which are directly emitted from sources, desert dust for example, and secondary aerosols, which are formed in the atmosphere from chemical and physical processes involving gaseous precursors. Secondary aerosols can be split into two types: Secondary Organic Aerosols (SOA) and Secondary Inorganic Aerosols (SIA). Gaseous precursors for SOA are Volatile Organic Compounds (VOCs), like isoprene for example, and correspond to a mixture of many different organic gases mainly composed of carbon, hydrogen and oxygen. Secondary inorganic aerosols' main precursors are the gaseous species: ammonia, nitric acid and sulfuric acid. The proportion of SIA in the Particulate Matter is generally significant. For example, in Europe, SIA represents between 30 and $50\,\%$ by mass of the $\mathrm{PM}_{2.5}$ (Querol et al., 2004). Ammonia comes from emissions, while nitric acid and sulfuric acid mostly result from the oxidation of nitrogen oxides and sulfur dioxide, respectively. SIA are therefore controlled by the emissions of ammonia, nitrogen oxides and sulfur dioxide, and also

by the ambient conditions, temperature and humidity. While typical sources of nitrogen oxides more varied (fossil fuel combustion, soils, biomass burning and lightning), sulfur compounds are mostly from anthropogenic sources and volcanoes (Seinfeld and Pandis, 1998). Ammonia emissions mostly come from domestic animals' excreta, synthetic fertilizers, biomass burning and crops (Olivier et al., 1998).

Gas phase aerosol interactions result in modifications of the gas phase equilibrium. Hydrolysis of N_2O_5 into HNO_3 on aerosols particles is an example. The nitric acid produced is more soluble and can then be deposited through wet deposition processes more easily than N_2O_5. Nitric acid can also condense in nitrate aerosols. This can potentially result in a decrease of NO_x, which can cause a decrease in O_3 concentrations up to 25% during spring (Dentener and Crutzen, 1993).

Modelling the aerosols is important at the local scale but also at the regional and global scales. At the local or regional scales, modelling the aerosols is a way to provide air quality forecasts for PM_{10} and $PM_{2.5}$. At the global scale, aerosols modelling is important for properly taking into account the long range transport of pollutants. It can also be used to study the evolution of the large scale background concentrations in current evolving climate conditions.

The representation of SIA in models simulating the composition of the atmosphere is, to our knowledge, always based on the assumption of an equilibrium between the gas and the aerosol phases both in global (Hauglustaine et al., 2014; Paulot et al., 2015) or regional models (Bessagnet et al., 2004; Vogel et al., 2009).

MOCAGE is the Chemical Transport Model (CTM) developed and used at CNRM/Météo-France. It is a global model that includes the capability for simulating smaller domains with finer resolutions. MOCAGE is used for simulating stratospheric and tropospheric chemical concentrations (ozone for example) and also for air quality forecasts including ozone, nitrogen oxides and aerosols. Recently, new developments have been made to account for the formation of secondary inorganic aerosols in MOCAGE. This SIA module is based on the gas-aerosol equilibrium assumption like in other models. It aims to be valid at different scales and resolutions since MOCAGE can simulate simultaneously the global and the regional scales thanks to grid-nesting. These new developments are aimed at being used for research purposes but also for

eventually being incorporated into operational systems. Therefore, choices were made to have, at first, a simple and computationally efficient module. The aim of this paper is to present and evaluate the MOCAGE SIA module both at the global and regional (European) scales.

Section 2 presents the MOCAGE model including the newly developed secondary inorganic aerosol module. Then in Sect. 3 we define the experimental setup of the simulations and the observations used for the model evaluation. Results are discussed in Sect. 4 for global simulations and Sect. 5 for regional simulations. Finally Sect. 6 concludes this study.

2 Model description

MOCAGE (*Modele de Chimie Atmospherique à Grande Echelle*) is an off-line global Chemistry Transport Model (CTM) used for research at Météo-France and serving in a wide range of scientific studies on tropospheric and stratospheric chemistry at various spatial and temporal scales. It was used for example for studying the impact of climate on chemistry (Teyssèdre et al., 2007; Lacressonnière et al., 2012; Lamarque et al., 2013) or tropospheric–stratospheric exchanges using data assimilation (El Amraoui et al., 2010; Barré et al., 2013). MOCAGE is also used for daily operational air quality forecasts in the framework of the French platform Prev'Air ((Rouil et al., 2009), http://www2.prevair.org/) and in the European MACC-III (Monitoring Atmospheric Composition and Climate) project by being one of the seven models contributing to the regional ensemble forecasting system over Europe ((Marécal et al., 2015), http://macc-raq-op.meteo.fr/index.php).

2.1 Model geometry and inputs

MOCAGE can be used both as a global model and as a regional model. Thanks to its two-way grid-nesting capacity, it can use several overlapping grids. The typical resolution at the global scale is 2° longitude $\times$ 2° latitude (approximately $220\,\mathrm{km} \times 220\,\mathrm{km}$ at the equator and $220\,\mathrm{km} \times 160\,\mathrm{km}$ at mid-latitudes), 0.5° longitude $\times$ 0.5° latitude at a regional scale (approx-

imately $55\,\mathrm{km} \times 40\,\mathrm{km}$ at mid-latitudes), and $0.1°$ longitude $\times$ $0.1°$ latitude at the local scale (approximately $11\,\mathrm{km} \times 8\,\mathrm{km}$ at mid-latitudes).

MOCAGE has 47 levels from the surface up to $5\,\mathrm{hPa}$. It uses σ-pressure vertical coordinates giving a non-uniform resolution of about $40\,\mathrm{m}$ in the lower troposphere increasing to $800\,\mathrm{m}$ in the upper troposphere. There are seven levels in the planetary boundary layer, twenty in the free troposphere and twenty in the stratosphere.

MOCAGE, being an off-line CTM, gets its meteorological fields from two possible independent meteorological models. Wind, temperature, humidity and pressure come from the IFS model (Integrated Forecast System) operated at ECMWF (European Centre for Medium-Range Weather Forecasts, http://www.ecmwf.int/) or from the ARPEGE model (*Action de Recherche Petite Echelle Grande Echelle*) operated at Météo-France (Courtier et al., 1991). The meteorological fields driving MOCAGE are available every 3 or 6 h, and are linearly interpolated on one hour intervals, one hour being the dynamical time step of the model.

The chemical time-step used in the solver varies with altitude from 15 min in the stratosphere to a few seconds in the planetary boundary layer. Emissions are injected every 15 min, into the five lowest levels using an hyperbolic decay. Chemical fields are then updated every 15 min.

2.2 Gaseous species

2.2.1 Current chemistry scheme

MOCAGE uses two chemical schemes in order to represent both the tropospheric and the stratospheric air composition. The Regional Atmospheric Chemistry Mechanism (RACM) (Stockwell et al., 1997) is used in the troposphere while the REPROBUS scheme is used for the stratosphere (REactive Processes Ruling the Ozone BUdget in the Stratosphere) (Lefèvre et al., 1994).

Compared with the initial RACM scheme, the sulfur cycle has been completed. Following Boucher et al. (2002) and Pham et al. (1995), MOCAGE takes into account the aqueous oxidation reaction of sulfur dioxide into sulfuric acid (Ménégoz et al., 2009; Lacressonnière, 2012). The fraction of gas dissolved in the liquid water content, the latter being a variable extracted from the input forcing fields, is calculated with Henry's law. The Henry's law constants for

H_2O_2, O_3 and SO_2 are respectively $7.45 \times 10^4 exp^{(7400(\frac{1}{T}-\frac{1}{298}))}$, $1.13 \times 10^{-2} exp^{(2300(\frac{1}{T}-\frac{1}{298}))}$ and $1.23 \times exp^{(2900(\frac{1}{T}-\frac{1}{298}))}$. SO_2 can then be oxidized by H_2O_2 and O_3. For H_2O_2, the reaction rate is given by:

$$\frac{dS}{dt} = \frac{k_1 \left[H^+\right] \left[H_2O_2\right] \left[HSO_3^-\right]}{1 + P\left[H^+\right]}, \tag{1}$$

where $k_1 = 7.5 \times 10^7 e^{-4430(\frac{1}{T}-\frac{1}{298})}$, T is the ambiant temperature and P the pressure. For O_3, the reaction rate is given by:

$$\frac{dS}{dt} = \left(k_2 \left[SO_{2aq}\right] + k_3 \left[HSO^-\right] + k_4 \left[SO_3^{2-}\right]\right) \left[O_3\right], \tag{2}$$

where $k_2 = 2.4 \times 10^4$, $k_3 = 3.7 \times 10^5 . e^{-5530(\frac{1}{T}-\frac{1}{298})}$ and $k_4 = 1.5 \times 10^9 . e^{-5280(\frac{1}{T}-\frac{1}{298})}$. The pH of the droplets, used to calculate the concentration of H^+ is supposed to always be equal to 5. This value is consistent with pH measurements from Charlson et al. (1982). This information is summarized in the Table 1, which gives the heterogeneous formation processes of the secondary inorganic aerosol precursors.

MOCAGE represents 111 gaseous compounds, 377 thermal gas reactions and 55 photolysis. Reaction rates are calculated during the simulation, every 15 min. The photolysis reactions rates are interpolated every 15 min from a lookup table and modulated by accounting at each given point and time for the ozone column, solar zenith angle, cloud cover and surface albedo.

2.2.2 New developments for gaseous species

Ammonia (NH_3) has been added to the model species in order to account for the formation of the ammonium aerosols. No extra gaseous reaction involving ammonia has been added since they are slow enough to be neglected (Adams et al., 1999).

Dentener and Crutzen (1993) showed that the hydrolysis reaction of N_2O_5 on aerosols surface plays an important role in the atmosphere by lowering NO_x and O_3 concentrations. It has

been added following Dentener and Crutzen (1993). The reaction rate is based on the available aerosol surface area, A, needed for the reaction to take place. The reaction rate is given by:

$$k_{N2O5} = \left(\frac{r}{G_g} + \frac{4}{v\gamma} \right)^{-1} A, \tag{3}$$

where D_g ($\mathrm{cm^2 s^{-1}}$) is the gas phase diffusion coefficient, r the aerosol radius, v the mean molecular speed ($\mathrm{cm\,s^{-1}}$), and γ the reaction probability being 0.1. Table 1 also includes this reaction.

2.3 Aerosols

2.3.1 Current aerosol module

The model in its current state is able to represent primary aerosols (Martet et al., 2009; Sič et al., 2015). The latest version of the primary aerosol scheme in MOCAGE has been evaluated by Sič et al. (2015). Sič et al. (2015) checked the aerosol physical parameterizations and proposed improvements. Based on simulations including only primary aerosols, they checked the consistency and validated the dry and wet deposition, the sedimentation and the emission processes. Concerning emissions, emission changes produced a strong impact by lowering known biases of sea salt and African dust. The wet deposition scheme changes also have a strong impact but they are more complex to analyse. Regarding sedimentation, changes produced a less important effect. Results obtained from Sič et al. (2015) confirm that the use of parameterizations can induce large uncertainties.

MOCAGE uses the sectional approach with six size bins per type of aerosol, especially chosen to fit the different characteristics of each aerosol. Primary aerosols in MOCAGE are composed of four species: desert dust, sea salt, primary organic carbon and black carbon. Black carbon and organic carbon emissions rely on emission inventories while sea salt and desert dust are dynamically emitted.

2.3.2 Emission parameterizations for aerosols

Desert dust and sea salt emissions are managed dynamically through parameterizations. Sea salt emissions are computed using Gong (2003) with a rate (particles $\mathrm{m}^{-2}\mathrm{s}^{-1}\mathrm{m}^{-1}$) given by:

$$\frac{dF}{dr} = 1.373 u_{10}^{3.41} r^{-A} \left(1 + 0.057 r^{3.45}\right) \times 10^{1.607 e^{-b^2}}, \tag{4}$$

where r is the particle radius at 80% relative humidity, u_{10} is the wind speed at 10m above the surface (ms^{-1}) and the parameters $A = 4.7\,(1 + 30r)^{-0.017 r^{-1.44}}$ and $B = (0.433 - log\,(r))\,/0.433$. This expression is modulated by the sea surface temperature in order to correct Gong (2003) formulation which overestimates sea salt emissions over cold water and underestimates them over warm water. The modified sea salt source function includes a sea surface temperature dependence (Jaeglé et al., 2011):

$$\frac{dF}{dr} = \left(0.3 + 0.1 T_s - 0.0076 T_s^2 + 0.00021 T_s^3\right) 1.373 u_{10}^{3.41} r^{-A} \left(1 + 0.057 r^{3.45}\right) \times 10^{1.607 e^{-b^2}}, \tag{5}$$

where T_s is the sea surface temperature. The emission spectrum is integrated over each bin range.

Desert dust emissions are dynamically managed using Marticorena and Bergametti (1995):

$$F = \alpha G, \tag{6}$$

where F is the vertical flux of desert dust aerosols, G is the horizontal flux of desert dust aerosols and α is a parameter depending on the soil specificity. The horizontal flux, G, is defined by:

$$G = EC \frac{\rho_a}{g} u^{*3} \int_{D_p} (1 + R) \left(1 - R^2\right) dS_{rel}\,(D_p)\, dD_p, \tag{7}$$

where E is the erodible fraction of the soil, C is a constant ($C = 2.61$), ρ_a is the density of the air, g the gravitational constant, D_p the particle size and u^* the friction velocity. R is defined by:

$$R = \frac{u_t^*}{u^*} \tag{8}$$

where u_t^* is the threshold friction velocity allowing particle emissions. The total emission is divided into the bins using 3 modes of mean number diameters $r_1 = 0.64\,\mu\mathrm{m}$, $r_2 = 3.45\,\mu\mathrm{m}$ and $r_3 = 8.67\,\mu\mathrm{m}$ of standard deviation $\sigma_1 = 1.7$, $\sigma_2 = 1.6$ and $\sigma_3 = 1.5$. Desert dust emission is available over Sahara and Eastern Asian desert.

Emissions of desert dusts and sea salts are calculated using the meteorological forcing at the resolution of each domain. Primary organic carbon and black carbon emissions are managed through emission inventories.

2.3.3 New developments of the aerosol module

In Sič et al. (2015), they only take into account primary aerosols that do not interact with each other. Therefore external mixing was assumed and each type of aerosols used specific size bins. To introduce SIA into MOCAGE, we assume aerosol internal mixing in order to represent interactions between aerosols. To implement internal mixing, we use a new set of bin sizes that are the same for all types of aerosols, ranging from $2\,\mathrm{nm}$ to $50\,\mu\mathrm{m}$ with size bin limits of: 2, 10, $100\,\mathrm{nm}$, 1, 2.5, 10 and $50\,\mu\mathrm{m}$. These new bin limits have been tested on a one year global simulation only with primary aerosols and compared to a similar simulation that used the aerosol specific size bins following Sič et al. (2015). The use of these new size bins gives similar results to when using the aerosol dependent ones with a resulting difference of less than $5\,\%$ on the estimation of PM_{10} and $\mathrm{PM}_{2.5}$ burden on the annual mean at the global scale. This new set of bins will become relevant when microphysical processes such as nucleation will be implemented in a futur version of the model.

From this basis, it was possible to introduce secondary inorganic aerosols in MOCAGE. SIA results from a partition between the gaseous phase and the aerosol phase. This partition depends on compound concentrations both in the gaseous and the aerosol phases and the ambient

conditions: temperature and humidity. This partition can be solved using a thermodynamic equilibrium model. We choose for this purpose to use the latest version of the thermodynamic equilibrium model called ISORROPIA II (Nenes et al., 1998; Fountoukis and Nenes, 2007) , which is used here in the deliquescent configuration. ISORROPIA is commonly used in state-of-the-art CTMs for instance in CHIMERE (Bessagnet et al., 2004) and LOTOS-EUROS (Schaap et al., 2008). Sulfate, nitrate and ammonium aerosol concentrations are simulated by ISORROPIA, each of these species being represented in MOCAGE with six concentrations for each of the six size bins. ISORROPIA gives the thermodynamic equilibrium between 12 liquid aerosol species (see Table 2), 9 solid aerosol species (see Table 3) and 3 gaseous compounds (see Table 4). Wexler and Seinfeld (1990) showed that the time constant to achieve the equilibrium ranges from a few seconds for high aerosol mass concentrations and small aerosol sizes to more than a day for low mass concentrations and large particle radii. Nevertheless, we assume in MOCAGE that the equilibrium is reached in the 15 min chemical update frequency for the following reasons. The aim of the model is to be used mainly for air quality, especially the forecast of PM_{10} and $PM_{2.5}$. According to Capaldo et al. (2000), the forecast of total PM_{10} and $PM_{2.5}$ using an equilibrium method is in good agreement with more complex methods including a dynamic method. According to the authors, nitrate aerosols, especially in the coarse mode are poorly represented in their simulations. They claim the nitrate underestimation is due, at least partially, to the lack of reaction with sodium chloride, which is taken into account here. Moreover, for the operational use of MOCAGE, it is important to have the lowest computational cost possible. The equilibrium approach is about 400 times faster than a dynamic method and about 12 times faster than a hybrid approach (Capaldo et al., 2000).

ISORROPIA outputs include the total concentrations of different solid, liquid or gaseous compounds (see Tables 2–4). The aerosol outputs from ISORROPIA then have to be distributed over the MOCAGE model size bins. The secondary inorganic aerosols are distributed in the bins as follows. We assume that the compounds related to sea salts, i.e., sodium and chlorine, are distributed with the same size distribution as the sea salt aerosol variables in the model. Sea salts are emitted with a specific size distribution. Their time evolution in the model modifies this distribution because of the different physical phenomena affecting sea salts such as sedimen-

tation (incorporating hygroscopicity) or wet and dry deposition. Thus, at a given point and at a given time, sea salts have a specific size distribution taking into account their evolution since the emission. ISORROPIA outputs including sodium or chlorine are distributed proportionally according to this specific distribution.

The other compounds are distributed following the measured accumulation mode for SIA from Zhuang et al. (1999) (see Table 5). The nuclei mode is not used because of the lack of the coagulation processes in the model allowing mass transfer from the condensation mode to the accumulation mode. Thus by distributing only into the accumulation mode, we implicitly assume that the coagulation has already been acting to transform fine mode aerosols into accumulation mode aerosols. The coarse mode is also not used because the formation of coarse particles through reaction with sea salts is treated separately (cf. explanations in the previous paragraph). The remaining coarse particles, are assumed negligible. Indeed, Zhuang et al. (1999) found that sulfate coarse mode is mainly due to reaction of sulfur dioxide on sea salts or soil particles and nitrate coarse mode is mainly due to reaction of gas phase HNO_3 with sea salts particles. The nitrate and sulfate fraction that reacts with sea salts is treated separately using the sea salt size distribution. Zhuang et al. (1999) also found that ammonia gas prefers to react in the fine mode. It forms coarse mode ammonium only if ammonia gas is present in excess to form ammonium chloride in sea salt.

For example, we can consider two forms of nitrate $NaNO_3$ and $(NH_4)_2SO_4$. $NaNO_3$ results from an interaction between nitric acid (HNO_3) and sea salts (NaCl), this is why some nitrate is split into size bins with the same proportions as the sea salts. $(NH_4)_2SO_4$ results from ammonia (NH_3) and sulfuric acid (H_2SO_4), then we will use measured modes from Zhuang et al. (1999) to distribute nitrate into the corresponding size bins.

In summary, the choice made here was to assume that each type of aerosol is distributed into its bins all along its lifetime following the defined modes (and associated parameters) based on observations published in the literature. By doing this, we assume that the defined modes already include all the aerosol microphysical processes implicitly. This is why nucleation and coagulation are not explicitly in the model. This simple approach, which has the advantage of

requiring low computation time, can be regarded as the first stage in the development of SIA in MOCAGE.

2.4 Transport and physical parameterizations

2.4.1 Transport

MOCAGE uses a semi-lagrangian advection scheme (Williamson and Rasch, 1989) to transport chemical species at the resolved scale. For the convective transport, the numerical model uses the parameterization of Bechtold et al. (2001). The species are diffused by the turbulent mixing in the planetary boundary layer as described by the scheme of Louis (1979).

2.4.2 Physical parameterizations for gaseous compounds

Dry deposition of gaseous compounds is taken into account following Wesely (1989). Dry deposition is calculated as follows:

$$F_{dg} = -v_d C \tag{9}$$

where F_{dg} represents the vertical dry deposition flux, v_d the deposition velocity of the considered compound and C its concentration. v_d is calculated using the concept of surface resistances in series as follow:

$$v_d = \frac{1}{R_a + R_b + R_c} \tag{10}$$

where R_a represents the aerodynamic resistance, R_b the quasi-laminar layer resistance and R_c the canopy resistance (Wesely, 1989). Wet deposition of gaseous species for the convective part is based on Mari et al. (2000) while the stratiform part from Liu et al. (2001) based on Giorgi

and Chameides (1986). Wet deposition is divided into two parts. The rainout is the process occuring when gases are dissolved into the droplets during their formation. It is also called in-cloud scavenging. When the droplets fall, they can collect some material. This process is called washout or below-cloud scavenging.

2.4.3 Physical parameterizations for aerosols

Dry deposition of aerosols and gravitational settling are implemented as described in Seinfeld and Pandis (1998). The dry deposition velocity is defined as:

$$V_{dd} = \frac{1}{R_a + R_b} + V_p, \tag{11}$$

where R_a is the aerodynamical resistance (sm^{-1}), R_b is the quasi-laminar layer resistance (sm^{-1}) and V_p is the settling velocity (ms^{-1}).

The settling velocity is based on Stokes' law and is a function of the particle diameter, particle density and air viscosity:

$$V_p = \frac{D_p^2 \rho_p g C_c}{18 \mu_a}, \tag{12}$$

where D_p is the ambiant aerosol diameter (m), taking into account hygroscopicity by computing a humid diameter. ρ_p is the aerosol particle density (kgm^{-3}), g is the gravitational constant (ms^{-2}), μ_a is the dynamical viscosity of air (Pas) and C_c is the slip correction factor which accounts for noncontinuum effects when the particle diameter and the air mean free path are of the same order of magnitude (Seinfeld and Pandis, 1998).

Aerosol wet deposition takes into account in-cloud scavenging (Giorgi and Chameides, 1986), below-cloud scavenging (Slinn, 1977) and below-cloud scavenging due to snowfall (Slinn, 1982). The fraction of aerosols removed at each time step by precipitation is calculated as:

$$F = f_{prec}\left(1 - e^{-\Lambda \Delta t}\right), \tag{13}$$

where F is the fraction of removed aerosols, f_{prec} is the fraction of precipitating cloud cover, Λ is the scavenging coefficient (s^{-1}) which describes a rate of loss of particles due to scavenging and Δt is the model time step for scavenging (s). The scavenging coefficient, Λ, consists of the in-cloud scavenging coefficient, Λ_{ro}, and the below-cloud scavenging coefficient due to rainfall, Λ_{wo}. To represent properly the precipitating cloud an estimation of the fraction of precipitation forming clouds is made for statiform and convective clouds. For statiform clouds, the fraction of precipitating clouds is given by:

$$f_{strat} = \frac{Q}{L_{st}.R_{st} + Q}, \tag{14}$$

where Q is the gridbox mean rate of precipitation formation including both liquid and solid precipitation ($kgm^{-3}s^{-1}$). L_{st} is the typical in-cloud liquid water content in precipitation forming stratiform clouds (Brost at al.,, 1991). R_{st} is the in-cloud rate constant for conversion of cloud water to precipitation for stratiform clouds. For convective clouds, the fraction of precipitating cloud cover within a gridbox for any given time step of the model (Δt) is:

$$f_{conv} = \frac{F_0 Q \frac{\Delta t}{t_c}}{Q \frac{\Delta t}{t_c} + F_0 R_{cv} L_{cv}}, \tag{15}$$

where F_0 is the maximum cumulus cloud cover assumed in the radiation calculations backed by observations, t_c is the typical duration of precipitation from a cumulonimbus cloud ($t_c = 30\text{min}$, Liu et al. (2001)). The in-cloud scavenging coefficient is different for stratiform and convective precipitation (Giorgi and Chameides, 1986). For stratiform precipitation, it is defined by:

$$\Lambda_{rost} = R_{st} + \frac{Q}{L_{st}}. \tag{16}$$

For convective precipitation it is:

$$\Lambda_{rocv} = R_{cv}. \tag{17}$$

Concerning below-cloud scavenging, the scavenging coefficient is defined as shown in Seinfeld and Pandis (1998):

$$\Lambda_{wo} = \frac{3}{2}\frac{E_r P}{D_d}, \tag{18}$$

where E_r is the collection efficiency of a raindrop to collect a particle during its fall. It is calculated following Slinn (1977). P is the precipitation rate ($\mathrm{kgm^{-2}s^{-1}}$) and D_d is the raindrop diameter (m). For more details on sedimentation and wet deposition of aerosols, see Sič et al. (2015).

3 Experimental setup and observations

3.1 Simulations

Two series of simulations are conducted in order to evaluate the developments to the model secondary inorganic aerosol scheme on the global and the regional scales. Two simulations were run at the global scale, at a resolution of 2° lon × 2° lat, for the year 2005. We chose the year 2005 because a large set of observations are available all over the world for this year. One of the simulations takes into account the newly integrated secondary inorganic aerosols (hereafter referred to as RACMSIA). The other one corresponds to the original version of MOCAGE without SIA (hereafter referred to as RACM). Simulations are run with a spin-up of 3 months and are driven by the meteorological fields from ARPEGE analyses.

The second series of simulations corresponds to a more recent period and focuses on the European domain to do an evaluation at the regional scale. Two simulations, with and without secondary inorganic aerosols, are conducted for the year 2010 and are compared to the EMEP measurement dataset. Both simulations have the global domain at 2° lon × 2° lat, and a nested European domain at 0.5° lon × 0.5° lat resolution. The latter domain covers the western part of the European continent between 16° W to 36° E and 32 to 72° N. The two domains communicate with each other by a two-way grid nesting scheme.

3.1.1 Gaseous and aerosol emissions

At the global scale, the IPCC/AR5 emissions are used, representative for the year 2000, for the anthropogenic species and biomass burning emissions (Lamarque et al., 2010). Biogenic emissions for gaseous species are based on GEIA. We used the inventory representative for 1990 but it was checked *a posteriori* on a two month period that the model performances are not significantly changed when using the recent MEGAN-MACC inventory (Sindelarova et al., 2013). Nitrous oxides from lightning are taken into account following Price et al. (1997). The IPCC/AR5 emissions for organic carbon and black carbon aerosols are used (Lamarque et al., 2010). This first set of emissions is used to simulate the year 2005 using a global domain.

At the regional scale, over the European continent, the MACC project emissions, representative for the year 2009, are used for anthropogenic gaseous compounds (Kuenen et al., 2014) and completed by GEIA emissions for biogenic sources. The MACC project emissions are also used for the aerosols (Kuenen et al., 2014). This second set of emissions is used for simulating the year 2010 over the Europe. At the global scale we use the same emissions as for the global simulation.

3.2 Observations for global simulation evaluation

MODIS daily mean AODs were used to evaluate the model simulations. For this purpose, we use the daily MODIS data level 3 (L3, collection 5.1) for the year 2005 and perform an additional quality control and screening as presented in Sič et al. (2015). This processing is done to minimize the number of observations that are cloud contaminated and those with statistically low confidence which often artificially increase AOD (Zhang et al., 2005; Koren et al., 2007; Remer et al., 2008). Moreover, Ruiz-Arias et al. (2013) showed there is a rapid increase of the relative underestimation of AODs when the MODIS' L3 AODs are below 0.1. We then perform an additional screening by rejecting all AOD values below 0.05. Below this value, the underestimation of AOD leads to a mean relative error higher than $50\,\%$ (Ruiz-Arias et al., 2013).

AODs in MOCAGE are calculated at $550\,\mathrm{nm}$ using Mie theory with refractive indices taken from Global Aerosol Data Set (Köpke et al., 1997) and extinction efficiencies derived with Wiscombe's Mie scattering code for homogeneous spherical particles (Wiscombe, 1980).

For the model evaluation, we also use the database made available by HTAP. It includes data from several measurement networks: EMEP, IMPROVE, NAtChem, EANET, CREATE, EUSAAR, NILU and the WMO-PCSAG global assessment precipitation dataset (http://www.htap.org/,http://www.ebas.nilu.no). We use observations of gaseous concentrations (nitric acid, nitric oxides, sulfur dioxide, ammonia), and the particulate matter composition (sulfate, nitrate, ammonium). The release used here is dated from 1 April 2014. Daily observations and weekly observations are used separately in order to consider comparisons at the same temporal scale. Daily observations cover both European countries and Canada. Weekly observations cover essentially the north of America and the eastern part of Asia. This is illustrated by Fig. 1 represents the location of the stations measuring SIA composition. It shows a good coverage of sulfate and nitrate measurements in the Northern Hemisphere. There are fewer ammonium aerosol measuring stations, with some zones that are not covered like the western part of the United States or some parts of Europe. Note also that the lack of ground observations in the Southern Hemisphere does not allow us to make the model evaluation in this part of the world, except for the comparison against MODIS AOD retrievals.

3.3 Observations for the model evaluation over Europe

The evaluation at the regional scale is split into two parts. The first part is based on the EMEP observation database and is aimed to check the good simulation of secondary inorganic aerosols. We use daily observations of concentrations. The second part is based on the AIRBASE observation database. It is aimed to check the performance of the model against air quality monitoring station observations on a hourly base.

3.3.1 EMEP database

The European Monitoring and Evaluation Programme (EMEP) is a scientifically based and policy driven programme under the Convention on Long-range Transboundary Air Pollution (CLRTAP) for international co-operation to solve transboundary air pollution problems (http://www.emep.int). Observations were downloaded through the EBAS repository (http://ebas.nilu.no). Daily observations are used to evaluate secondary inorganic aerosol composition (sulfate, nitrate, ammonium) over Europe. Figure 2 represents the location of the stations measuring SIA composition on a daily basis. One can note similar remarks as for the measurements shown in Fig. 1 with a good coverage of sulfates and nitrates measurements and to a lower extent for ammonium measurements. Nevertheless, some areas, in France for example, are not very well covered. The EMEP monitoring sites are located such that significant local influences are minimised (Tørseth et al., 2012). Therefore measurements are assumed to be directly comparable to model outputs which here are at $0.5^\circ \times 0.5^\circ$.

3.3.2 AIRBASE database

To make a complementary evaluation, and because SIA directly affects major regulated air pollutants, we also make comparisons with air quality indicators monitored over Europe. For this we use AIRBASE, which is a dense measurement network used for air quality issues. It is managed by the European Topic Centre on Air Pollution and Climate Change Mitigation on behalf of the European Environment Agency. For this study, we use the latest version (version 8) of the AIRBASE database (http://acm.eionet.europa.eu/databases/airbase). AIRBASE data are used in this study to evaluate the performance of the model for PM_{10}, $PM_{2.5}$, ozone and nitrogen dioxide. For 2010, a total of 38 countries, including the 27 European Union countries have provided air quality data.

AIRBASE measuring stations are located on various sites: urban, periurban, rural, etc. In order to be able to compare the model simulations at the 0.5° longitude $\times$ 0.5° latitude resolution, we select the stations which are representative of the model resolution. Following Joly and Peuch (2012), each station is characterised with a class between 1 and 10 according to its statisti-

cal characteristics, 1 corresponding to a fully rural behaviour and 10 to a highly polluted station. The selection of stations is done following Lacressonnière et al. (2012) who conducted an evaluation of MOCAGE at the regional scale over several years. Only the stations corresponding to 1 to 5 classes are kept for ozone. For nitrogen dioxide, only the station corresponding to 1 and 2 classes are kept since nitrogen dioxide is a short lived species. For PM_{10} we select the stations with classes ranging from 1 to 5. Joly and Peuch (2012) do not provide a classification for $PM_{2.5}$. We choose to use the same stations for $PM_{2.5}$ as for PM_{10}.

3.4 Metrics used for evaluation

Several statistical indicators can be used for model evaluation against in situ data. Seigneur et al. (2000) state that past model performance evaluations have generally used observations to normalize the error and the bias. This approach can be misleading when the denominator is small compared to the numerator. Following Seigneur et al. (2000), we chose to use the fractional bias and the fractional gross error instead of the bias and the root-mean-square error (rmse).

The fractional bias, also called modified normalized mean bias (MNMB) or mean fractional bias (MFB), used to quantify, for N observations, the mean between modeled (f) and observed (o) quantities is defined as follow:

$$\text{MNMB} = \frac{2}{N}\sum_{i=1}^{N}\frac{f_i - o_i}{f_i + o_i} \tag{19}$$

The fractional bias ranges between -2 and 2 varying symmetrically with respect to under and overestimation.

The fractional gross error (FGE), also called mean fractional error (MFE) aims at quantifying the model error. It varies between 0 and 2 and is defined by:

$$\text{FGE} = \frac{2}{N}\sum_{i=1}^{N}\left|\frac{f_i - o_i}{f_i + o_i}\right| \tag{20}$$

The correlation coefficient r indicates the extent to which patterns in the model match those in the observations and is defined by:

$$r = \frac{\frac{1}{N}\sum_{i=1}^{N}\left(f_i - \overline{f}\right)\left(o_i - \overline{o}\right)}{\sigma_f \sigma_o} \tag{21}$$

Where σ_f and σ_o are standard deviation respectively from the modelled and the observed time series and $\overline{f}$ and $\overline{o}$ their mean values.

Boylan and Russell (2006) give criteria to characterize a model performance against observations based on MNMB and FGE. It gives two types of performance. The "performance goal" is the level of accuracy that is considered to be close to the best a model can be expected to achieve. The "performance criteria" is the level of accuracy that is considered to be acceptable for modelling applications. For example, for particulate matter, for stations having a mean concentration superior to $2.25\,\mu\mathrm{g\,m^{-3}}$ the "performance goal" is reached when the MNMB and the FGE are equal or less than ± 0.3 and 0.5 respectively. These recommendations depend on the mean concentration of an observation point (see Table 1 in Boylan and Russell, 2006). In particular, less polluted stations might have large errors for MNMB and FGE but still be satisfactory.

4 Results and evaluation of the global simulations

This section presents results at the global scale. Firstly, we show and discuss the global concentrations before comparing results with measurements.

4.1 Global concentrations

Figure 3 represents the annual emission of the SIA precursors: sulfur dioxide, nitrous oxides and ammonia. The zones with highest emissions are mostly in the Northern Hemisphere located in the eastern part of Asia, North America and Europe. Ammonia emissions are larger in Europe and Eastern Asia than in North America. Ammonia and nitrous oxides also have high emissions in South America and Africa albeit to a lesser extent.

Figure 4 shows annual mean surface concentrations of the secondary inorganic compounds: sulfate, nitrate, ammonium and the sum of all these components. These fields are consistent with the emissions. High concentration zones correspond to zones of high emissions of precursors, being Europe, Eastern Asia and North America. However North American concentrations are slightly lower than the other areas of high concentrations. This might be due to the emissions of ammonia which are lower, being then less able to form aerosol with sulfate and nitrate. These mean annual secondary inorganic aerosol concentrations from MOCAGE are globally consistent in terms of geographical distribution and concentration values with Hauglustaine et al. (2014) model fields representative for 2000.

Figure 5 represents the comparison of HNO_3 and NH_3 annual mean concentrations between the RACM and the RACMSIA experiments. In the RACM experiment, ammonia does not chemically react. Dry and wet deposition are the only removal processes in this configuration. Ammonia is thus accumulating over time in the model's atmosphere. This is why there are very large differences between RACM and RACMSIA for NH3 leading to important changes also for HNO3. In the RACMSIA experiment, ammonia can take part in aerosol production under favorable conditions (thermodynamic and availability of other inorganic compounds). The ammonia field in RACMSIA is more consistent than RACM with the modelling results from Xu and Penner (2012).

For HNO_3, there is $200\,\mathrm{pptv}$ less HNO_3 in the RACMSIA experiment than in the RACM experiment. In the RACM experiment, geographic patterns agree with Xu and Penner (2012), but concentrations are overestimated. In the RACMSIA experiment, part of the nitric acid is transformed into aerosol and nitric acid concentrations are therefore lower and more consistent with Xu and Penner (2012).

4.2 Comparison to MODIS AOD

Figure 6 presents the 2005 annual modified normalized mean bias against MODIS AOD observations. In Fig. 6, one can see that the Northern Hemisphere has a negative MNMB globally between -1 and -0.5 in the RACM experiment. In the RACMSIA experiment it is closer to 0 (between -0.5 and 0.5). This shows an improvement of the model AOD at the global scale when

including SIA. This is confirmed by the global mean MNMB which is -0.41 for the RACM experiment and -0.21 for the RACMSIA experiment. Sič et al. (2015) made a similar comparison for primary aerosols only: AOD against MOCAGE simulations. They conclude their study by stating that one reason of MOCAGE negative bias in AOD might be due to the lack of secondary aerosols in their model version. Here we show that adding secondary inorganic aerosols improves MOCAGE results. The global modified normalised mean bias generally remains negative. A negative bias is expected over Asia, western Europe, eastern US and central Africa since the secondary organic aerosols are still missing in the model and are expected to be important in these areas (Tsigaridis and Kanakidou, 2003; Heald, C. L., et al., 2008). The AOD bias over central Asia is likely not only due to the lack of SOA but also to an underestimation of the dust emissions in this region. MOCAGE includes desert dust emissions over Eastern Asia but the large uncertainties of the wind fields over this region due to complex orography produce large uncertainties on desert dust emissions. Over ocean, there are no DMS emissions in the model and thus we expect AOD underestimation instead of overestimation. The positive bias over the ocean is likely due to the sea salt aerosols. The function used to calculate the sea salt emissions follows an exponential curve for big particles. These big particles remain in the atmosphere for a very short time and very close to the surface but are often emitted in the model. The model AOD overestimation can be linked to an uncertainty on the exponential emission function that possibly gives too many big particles. Also the AOD measurements may not capture the transient presence of big particles in the very low levels.

When comparing Fig. 6 with Fig. 4 one can notice that areas where AODs are increased correspond to areas where secondary inorganic aerosol concentrations are the most important, i.e. in Europe, Asia and Eastern part of North America. Near the coasts, where the influence from land is stronger, the bias is negative in the RACM experiment and is closer to zero by taking into account secondary inorganic aerosols (RACMSIA). In the Guinea Gulf, the improvement is noteworthy but the MNMB is still negative. This could be due to insufficient biomass-burning aerosol emissions, especially through secondary organic aerosol formation, or due to too low desert dust aerosol emissions. The large negative biases in both simulations on the western coast of South and North America can be linked to dust emissions missing over

these regions in MOCAGE, when comparing to the AEROCOM intercomparison project results (http://aerocom.met.no/.)

4.3 Atmospheric chemical composition against observations from the HTAP database

In this section, we use the daily observations as one time series to calculate the statistics. This allows us to give the same weight to every observation instead of every measuring station because measuring stations do not always provide the full set of observations for the whole year.

Modelled fields are interpolated to the observation location. We take the concentration at the surface, knowing that the altitude difference between the model and the actual station altitude can lead to significant differences. This is why stations with an altitude difference higher than $1000\,\mathrm{m}$ with the model orography have been suppressed for the statistics. After this screening, there are 98 stations left on daily observations (104 before screening). For weekly observations, there are 214 stations left (225 before screening).

4.3.1 Daily observations

Table 6 presents the statistical results against daily observations for the main components of the secondary inorganic aerosols: sulfate, nitrate and ammonium. As presented in Fig. 1 this type of observations is mainly located in Europe and Canada. Sulfate measurements are divided into two parts, sulfate total and sulfate corrected. The sulfate corrected corresponds to non sea salt sulfate (nss). The use of non sea salt sulfate is better for our comparison because we do not take into account the emission of sulfates being a part of sea salt aerosols. But to have the largest number of stations, we use both measures. In order to improve the comparison, we suppose that 7.68% of the mass of sea salt aerosols is composed of sulfates. This value corresponds to the proportion of sulfate in the sea water (Seinfeld and Pandis, 1998). For all the comparisons, the sulfate total measurements are then compared to the sulfate field of the model to which we added a fraction of the sea salt aerosol field.

Sulfate totals are well simulated, with a MNMB of 0.05. With a correlation of 0.33, and a FGE of 0.94, the model performs fairly. Observations corrected for sea salt sulfate compare

better with the model with a correlation of 0.70. The model slightly underestimates sulfate with a MNMB of −0.12. Ammonium is slightly overestimated with a MNMB of 0.19, and with a good correlation of 0.69. Nitrate is also well modeled with a low MNMB of 0.13, a fairly good correlation (0.53) but with a relatively high FGE (0.94).

The model is able to well simulate the time-series at a given point. As an example, Fig. 7 shows the time-series of corrected sulfate, nitrate and ammonium daily observations against MOCAGE values at an Irish measuring station. We choose this rural station because it is not under direct urban activity and it samples chemical export from North America. Therefore it measures background concentrations that can be compared to the model coarse resolution and these concentrations are not very low and have variations because of the North American export. The model performs well on the three components by capturing the daily variations and their values. Statistics over this station are given in Table 7. MOCAGE is able to represent well the SIA components with low MNMB and FGE and good correlations. Results for another station in Canada are presented in Table 8 while the time-series of sulfate, nitrate and ammonium daily observations against MOCAGE values are presented in Fig. 8. Observations of total sulfate are presented here, using the correction to account for the sea-salt origin sulfate. The RACMSIA simulation for this station has lower performances than for the Irish station. This can be explained for different reasons. Firstly one can note that the Fig. 8 shows the model is able to reproduce the different pollution episodes. The concentrations of secondary inorganic aerosols are nevertheless underestimated, except during winter time. The mean flux in winter and in summer comes from the Western part of Canada and from the Central United-States of America, respectively. As presented in Fig. 3 emissions are at a maximum in the Eastern part of the United States. In summer there is more pollution importation at the measuring station considered here. This importation can be underestimated due to the resolution of the model which is about 200km in this region implicating a mixing of the emissions in the model gridbox on one hand and a diffusion of the pollution plume.

We also checked the behaviour of the model against the diagnostic proposed by Boylan and Russell (2006), i.e., "performance goal" and "performance criteria". As expected, sulfate corrected, all of the 21 stations are well modelled according to both criteria. Sulfate totals are not

as well represented by the model, out of 94 stations, 5 do not comply with the "performance criteria" and 14 do not respect the "performance goal". For nitrate, only 2 stations do not respect both diagnostics over a set of 61 stations. There are 51 stations measuring ammonium concentrations and only 6 stations do not fit the "performance goal" while all do for the "performance criteria". The Boylan and Russell (2006) perspective confirms the good performance of the model for secondary inorganic aerosols compounds.

Table 9 presents the statistics for gaseous precursors of SIA both for RACM and RACMSIA experiments. Sulfur dioxide is not really affected by the SIA because there are no direct reactions newly integrated in the model. Oxidation of sulfur dioxide into sulfate was already taken into account in the RACM simulation (see section 2.2.1). But the scores for ammonia are significantly improved. The correlation rises from 0.18 to 0.33, the fractional gross error drops from 1.84 to 1.27 and the modified mean mean bias from 1.84 to 0.79. The nitrogen dioxide statistics are slightly better with the fractional gross error which decreases from 0.83 to 0.77 with SIA formation. Nitric acid seems better simulated with SIA formation looking at the MNMB, but the fractional gross error and the correlation are worse in the RACMSIA simulation including secondary inorganic aerosols. Depending on atmospheric conditions, SIA formation can be either a sink or a source of nitric acid. Also nitric acid undergoes many other processes that drive its concentration. Therefore simulating nitric acid variations with time and space is challenging and is not only related to the ability of the model to produce realistic SIA. This is why it is difficult to interpret nitric acid performances.

In summary on daily data, concerning Europe and Canada, the model is able to well simulate secondary inorganic aerosols. We note that the model tends to overestimate ammonium and ammonia. There is also an overestimation of sulfur dioxide while sulfates are slightly underestimated. Nevertheless these comparisons show the ability of the model to reproduce secondary inorganic aerosols at a global scale. It also shows than on a specific location the model is able to reproduce very well the SIA concentrations and their temporal evolution.

4.3.2 Weekly observations

Table 10 presents the statistical results against weekly observations for the main components of secondary inorganic aerosols. As presented in Fig. 1, weekly observations are mainly located in North America and Asia, so this type of observation is complementary to the daily ones. For sulfate, one can see that sulfate totals are well simulated with a MNMB of -0.05 and a correlation coefficient of 0.64. The results for the sulfate corrected observations should not be interpreted as a general behaviour because there is only one measuring station in this case. As for daily observations, ammonium is overestimated with a MNMB of 0.34 and a FGE of 0.84. Similarly for daily observations, the nitrate MNMB is low with a similar FGE of 1.00. As for the daily observations, the bias is low but the error is fairly high.

For gaseous compounds, statistics are not presented here because there are only between 16 and 28 stations depending on the parameter and there are no nitrogen dioxide measurements. Nevertheless the behaviour for this limited number of stations is similar to that of the daily observations.

Figure 1 presents the location of the stations used in this study. By looking at the weekly station localisation, one can see that there are two main groups of stations, one in North America and one in Asia. By splitting the dataset between Asian and American stations, there are 29 stations for the Asian area and 156 for the American one. The results are presented in Table 11.

Sulfates, based on total sulfate data, have a similar MNMB in both zones. The correlations too are similar for both continents (65 in North America and 64 in Asia). Nitrates are better simulated in North America. Indeed, MNMBs are 0.30 and 0.05 in Asia and North America, respectively. Moreover, the correlation is also better (0.41) than in Asia (0.13). MNMB of ammonium is also worse in Asia (0.35) than in North America (0.27). Nevertheless, the correlation of ammonium is better in Asia (0.41) compared to North America (0.19).

When comparing Figs. 1 and 6 one can observe that North American stations are located on areas where the model underestimates the AOD when simulating SIA while the Asian stations are located on areas where the AODs are well simulated by the model when taking into account SIA. When looking at stations in North America, comparisons to in situ measurements shows

a good agreement for SIA fields. The negative bias on Fig. 6 over this area might then be due to the lack of secondary organic aerosols in the model. The Asian stations comparisons however shows an overestimation of SIA. The good results on AOD comparison might there be due to an overestimation of SIA in this area compensated by an underestimation linked to the lack of SOA.

5 Results and evaluation of the regional simulation

The first set of simulations showed that the model was able to simulate correctly SIA on the global scale. The next step is to check the behaviour of the model over a regional domain, Europe, with a better resolution and different emission inventories.

This section presents results on the second set of simulations over the year 2010 including two nested domains: the global one (at 2° lon $\times$ 2° lat) and a regional one (at 0.5° lon $\times$ 0.5° lat). As we already looked at model results at a global scale (see Sect. 4), the focus in this section is put on the regional European domain. Firstly, we analyse the results before comparing them with measurements from the EMEP database for secondary inorganic aerosol components. Then we make a comparison to AIRBASE measurements from an air quality point of view.

5.1 European concentration fields

Figure 9 presents SIA precursor emissions (SO_2, NO_x and NH_3) for the year 2010 on the regional domain. SO_2 emissions are at a maximum in an area covering the Benelux, England and Central Europe. NO_x emissions are significant almost everywhere in Western Europe but with a maximum emission in Benelux and England. NH_3 is emitted everywhere except in Scandinavia with maxima in Brittany (France), Benelux and the Po Valley (Italy).

Figure 10 presents the annual mean surface concentration for the year 2010 over the regional domain. SIA are present almost everywhere especially over the continent, with very high concentrations in the Po valley, Benelux and Central Europe.

Sulfate aerosols are mainly present in Central Europe. This is due to the high emission zone of SO_2 in this region. These results are consistent with Schaap et al. (2004) who simulated the year 1995. Schaap et al. (2004) also found high sulfate concentrations over Benelux and England. There are no high sulfate concentrations over these locations in our simulation. These differences are due to the emission reduction program. Indeed Western Europe has strongly decreased its SO_2 emissions since 1995.

Nitrate aerosols are mainly present in Benelux and the Po Valley. Benelux has high nitrate concentrations due to high NO_x emissions in this area, while the Po Valley has not such high NO_x emissions, but a climate and a topography which favours pollution events.

Ammonium aerosols are less important in terms of mass concentration and are more smoothly distributed over the domain. Ammonium is present where either sulfate or nitrate are present, because the main SIA components are ammonium sulfates and ammonium nitrates.

Figure 11 presents the comparison of HNO_3 and NH_3 annual mean concentrations between the RACM and the RACMSIA experiments. Similarly to the global simulation, HNO_3 and NH_3 concentrations are lowered in the RACMSIA experiment compared to the RACM experiment. Compared to Schaap et al. (2004) NH_3 concentrations are too high in the RACM experiment while having closer values in the RACMSIA experiment. Patterns are also similar except for the Po Valley where both MOCAGE simulations show very high concentrations of ammonia. Concerning HNO_3, patterns are the same for both experiments.

5.2 Atmospheric chemical composition over a regional domain against EMEP observations

For this part, the observations are used in the same way as for the global scale. However here we only use daily observations because there are very few weekly observations (between 3 and 5 stations depending on the parameter observed).

Table 12 presents the statistical results for the main components of the secondary inorganic aerosols: sulfate, nitrate and ammonium. Sulfate, both total and corrected, are underestimated with an MNMB of -0.16 and -0.35 respectively and a FGE of 0.67 and 0.73. Correlation

is slightly better (0.68) for corrected sulfate than for total sulfate (0.57). Ammonium is only slightly overestimated, with an MNMB of 0.18, and is well modelled with a correlation of 0.71.

Table 13 presents the statistics for the gaseous precursors of SIA. The model has a similar behaviour as on the global scale against the daily observations from the HTAP database. In both simulations, the species with the best perfomances is NO_2 while the one with the worse scores is NH_3. The use of SIA mainly affects NH_3 with a very significant improvement of all statistical indicators. The differences between the model results and the observations can partly be explained by uncertainties in the emission inventories used. In (Kuenen et al., 2014), they report uncertainties in ammonia emission of about 50 %. For NO_x, uncertainties are lower but still about 30 %. SO_2 only has about 10 % uncertainty. These uncertainties in emission might explain differences for species ammonia, ammonium and for nitrogen dioxide. For sulfur compounds, there is an underestimation of sulfate aerosols and a strong overestimation of SO_2, which can not be explained only by the emission uncertainties. The oxidation process transforming SO_2 into sulfuric acid depends on several variables (gaseous concentrations, liquid water content, temperature, etc). It is therefore more difficult to represent it correctly since all these variables have also some associated uncertainties.

5.3 Air quality indicators

In order to complete the validation, we check the change on air quality pollutants due to the introduction of secondary inorganic aerosols. These indicators are surface concentrations of O_3 and NO_x (NO and NO_2) for gaseous species and PM_{10} and $PM_{2.5}$ for aerosols.

We also examine the impact of the seasonal basis, which is based on the statistics from three seasons: spring (March, April and May), summer (June, July, August) and fall (September, October and November). Winter is not analyzed here because winter months (December, January and February) are not simulated as a continuous series.

5.3.1 Particulate matter simulation: $PM_{2.5}$ and PM_{10}

Table 14 presents statistics for $PM_{2.5}$ over Europe for the year 2010 based on AIRBASE hourly observations. One can see that $PM_{2.5}$ is better represented in the RACMSIA version. Indeed, MNMB increases from -0.58 in RACM to -0.14 in RACMSIA and the FGE decreases from 0.77 in RACM to 0.56 in RACMSIA. MOCAGE still underestimates $PM_{2.5}$, but the error is smaller with the new version of the model with SIA. The correlation also rises from 0.47 to 0.58. Secondary organic aerosols are still missing in the model and likely explain the $PM_{2.5}$ negative bias. Table 14 also presents the statistics for PM_{10} over Europe for the year 2010 based on AIRBASE hourly observations. The conclusions for PM_{10} are similar to those of $PM_{2.5}$ but with slightly poorer statistics.

Table 15 presents the variation of $PM_{2.5}$ MNMB according to the season. The Δ represents the improvement of the RACMSIA experiment compared to the RACM experiment. Since the MNMB are all negative, a positive value of Δ means that adding secondary inorganic aerosols has a positive effect on the simulation.

Over the whole year, the MNMB is improved by 0.44. By looking at the behaviour on the different seasons, one can see than in spring (MAM) the improvement of $PM_{2.5}$ forecasts is larger than for the other seasons (0.52). When taking a look to the PM_{10} seasonal variability, the conclusion is the same. This behaviour is due to the fact that spring, especially March and April, is the most favourable period for secondary inorganic aerosols formation in Europe. In Summer, the MNMB is improved by 0.35 in the RACMSIA simulation, which is very significant. But the normalised bias in RACMSIA experiment is higher than for the other seasons. This is due to the fact that summer is a season favourable to secondary organic aerosol, still lacking in our model, especially with a biogenic origin. Indeed, biogenic volatile organic compounds such as isoprene for example, have higher emissions in summer which leads to higher biogenic secondary organic aerosols in summer.

5.3.2 Feedback on the gaseous chemistry

Figure 12 represents the annual mean concentrations of surface ozone for the RACM and the RACMSIA experiments. One can see a significant decrease in surface ozone, especially over oceans, between 5 and 10 ppbv. On land, concentrations are nearly the same. By being absorbed into the aerosol phase, nitric acid is not available for forming NO_x again and then the ozone equilibrium is displaced. The effect is less important over the land because of the proximity of NO_x sources which drive its concentrations.

Table 14 presents the statistics for ozone against hourly observations from the AIRBASE database. The statistics are very similar between the two experiments, only the MNMB is slightly better for the RACMSIA experiment. It is linked with the ozone maps showing a decrease over the ocean while the field is similar over land. Although the ozone maps show a decrease over the ocean the field is similar over land where the AIRBASE stations are located.

Table 14 presents the statistics for nitrogen dioxide against hourly observations from the AIRBASE database. All statistical indicators are close in both experiments (RACM and RACMSIA) indicating that the NO_2 equilibrium in MOCAGE is not affected by the introduction of SIA in the model. The comparison between Tables 13 and 14 shows that the MOCAGE simulations have similar performances against EMEP and AIRBASE. For these statistics we use 44 EMEP stations and 610 AIRBASE stations. This shows that the MOCAGE model with or without SIA provides robust NO_2 fields at the surface even when compared to a large number of data.

6 Conclusions

In this study we developed a secondary inorganic aerosol module into the CTM MOCAGE. These developments were made with the objectives of having a simple and computationally efficient module able to give good results while being able to be used in an operational framework and of being valid at different scales. We showed that the model is able to represent secondary inorganic aerosols on both the global scale and the European regional scale. The different constituents of the secondary inorganic aerosols being sulfate, nitrate and ammonium simulated

by the model fit well against the different observational datasets used. These databases and the AIRBASE database were also used to assess gaseous species concentrations. Comparisons show a neutral impact of SIA on SO_2 and NO_2, a mixed impact on HNO_3 (with a much better MNMB but slightly worse FGE and correlation) and a large improvement of NH_3. Simulations with SIA do not show a significant improvement on statistical scores for ozone. Nevertheless, there is an impact on ozone fields at the surface over the sea that is significant but very little change over land as reflected by the scores. The comparison with satellite AODs shows that the global aerosol budget is significantly better when SIA are used in the model. Finally, the model is able to perform generally very well at reproducing daily variations of SIA as illustrated by the comparison between MOCAGE and observations at a station in Ireland.

By comparing the MOCAGE model results to the AIRBASE dataset over Europe in terms of particulate matter concentration, we also showed that the model performs better with the introduction of secondary inorganic aerosols. Especially in spring (March, April, May), the MNMB of the $PM_{2.5}$ is improved by 0.52 rising from -0.55 to -0.03. Over the full year of simulation, there is still a negative bias in $PM_{2.5}$ and PM_{10} concentrations, which can be due to the lack of secondary organic aerosols in the model. The implementation of secondary organic aerosols in MOCAGE is the next major development foreseen to fully complete the aerosol scheme.

Model simulations with SIA show that SO_2 is significantly overestimated and the sulfates are underestimated. For instance at the regional scale, the SO_2 MNMB is 1.15 and the sulfates' MNMB is -0.36. This indicates that the model is not able to fully convert SO_2 into sulfate. This can be related to several sources of uncertainty within the conversion process such as temperature, liquid water content and its pH and gaseous concentrations of precursors that are partly linked to their emissions (Kuenen et al., 2014). Some work will be done in the future to identify the main sources of uncertainties in order to improve the representation of the SO_2 oxidation process into sulfuric acid. Concerning ammonia and ammonium, they have both positive bias that can at least be partly explained by the large uncertainties in ammonia emissions of about $50\,\%$ (Kuenen et al., 2014).

In the implementation, we made choices for representing phenomena favouring computational efficiency over a very detailed representation while keeping a good accuracy. There are weaknesses in this SIA module which could be improved. Firstly, all the microphysical processes have been treated implicitly in a very simple way. A next step would be to include them using physical parameterizations. In particular, nucleation, condensation and coagulation which are very important for the time evolution of the aerosol sizes. Another aspect to work on is the thermodynamic equilibrium hypothesis which leads to uncertainties. To improve this, it is necessary to account for the kinetics of the transfer between the gas phase and the aerosol phase, especially for big particles (Wexler and Seinfeld, 1990; Capaldo et al., 2000). A third improvement would be to take into account the formation of secondary organic aerosols in order to have the complete range of atmospheric particles and be able to represent properly the different interactions and impact of aerosols. One of the final goals is to integrate this module for operational forecasts into the Prev'Air and the COPERNICUS programs. The model MOCAGE will also be used to make research studies including long run simulations for instance for the CCMI program (Chemistry–Climate Model initiative) and the analysis of the aerosol budget in the Mediterranean area.

Code availability

This paper is based on source code that is presently incorporated inside the MOCAGE model. The MOCAGE source code is the property of Météo-France and CERFACS, and it is based on libraries that belong to some other holders. The MOCAGE model is not open source and routines from MOCAGE cannot be freely distributed. Therefore, we cannot provide the code openly to the GMD website.

Acknowledgements. We would like to thank Athanasios Nenes for providing us the ISORROPIA II source code (http://www.isorropia.eas.gatech.edu/). This work has been possible thanks to the AIRBASE, EMEP, HTAP database and EBAS database infrastructure. We also acknowledge the MODIS mission team and scientists for the production of the data used in this study

References

Adams, P. J., Seinfeld, J. H., and Koch, D. M.: Global concentrations of tropospheric sulfate, nitrate, and ammonium aerosol simulated in a general circulation model, J. Geophys. Res.-Atmos., 104, 13791–13823, 1999.

Barré, J., Peuch, V.-H., Lahoz, W., Attié, J.-L., Josse, B., Piacentini, A., Eremenko, M., Dufour, G., Nedelec, P., von Clarmann, T., and El Amraoui, L.: Combined data assimilation of ozone tropospheric columns and stratospheric profiles in a high-resolution CTM, Q. J. Roy. Meteor. Soc., 140, 966–981, 2013.

Bäumer, D., Vogel, B., Versick, S., Rinke, R., Möhler, O., and Schnaiter, M.: Relationship of visibility, aerosol optical thickness and aerosol size distribution in an ageing air mass over South-West Germany, Atmos. Environ., 42, 989–998, 2008.

Bechtold, P., Bazile, E., Guichard, F., Mascart, P., and Richard, E.: A mass-flux convection scheme for regional and global models, Q. J. Roy. Meteor. Soc., 127, 869–886, 2001.

Bessagnet, B., Hodzic, A., Vautard, R., Beekmann, M., Cheinet, S., Honoré, C., Liousse, C., and Rouil, L.: Aerosol modeling with CHIMERE – preliminary evaluation at the continental scale, Atmos. Environ., 38, 2803–2817, 2004.

Boucher, O., Pham, M., and Venkataraman, C.: Simulation of the Atmospheric Sulfur Cycle in the Laboratoire de Météorologie Dynamique General Circulation Model: Model Description, Model Evaluation, and Global and European Budgets, Scientific note from the IPSL Institut Pierre-Simon Laplace 21, 2002.

Boylan, J. W. and Russell, A. G.: {PM} and light extinction model performance metrics, goals, and criteria for three-dimensional air quality models, Atmos. Environ., 40, 4946–4959, doi:10.1016/j.atmosenv.2005.09.087, 2006.

Brost, R. A., Feichter, J., and Heimann, M.: Three-dimensional simulation of Be in a global climate model, Journal of Geophysical Research: Atmospheres (1984–2012), 96(D12), 22423–22445, 1991.

Capaldo, K. P., Pilinis, C., and Pandis, S. N.: A computationally efficient hybrid approach for dynamic gas/aerosol transfer in air quality models, Atmos. Environ., 34, 3617–3627, 2000.

Charlson, R. J., and Rodhe, H.: Factors controlling the acidity of natural rainwater. Nature, 295(5851), 683–685, 1982.

Courtier, P., Freydier, C., Geleyn, J., Rabier, F., and Rochas, M.: The ARPEGE Project at Météo-France, ECMWF workshop, European center for Medium-Range Weather Forecast, Reading, England, 1991.

Dentener, F. J. and Crutzen, P. J.: Reaction of N_2O_5 on tropospheric aerosols: impact on the global distributions of NO_x, O_3, and OH, J. Geophys. Res.-Atmos., 98, 7149–7163, 1993.

El Amraoui, L., Attié, J.-L., Semane, N., Claeyman, M., Peuch, V.-H., Warner, J., Ricaud, P., Cammas, J.-P., Piacentini, A., Josse, B., Cariolle, D., Massart, S., and Bencherif, H.: Midlatitude stratosphere – troposphere exchange as diagnosed by MLS O_3 and MOPITT CO assimilated fields, Atmos. Chem. Phys., 10, 2175–2194, doi:10.5194/acp-10-2175-2010, 2010.

Fountoukis, C. and Nenes, A.: ISORROPIA II: a computationally efficient thermodynamic equilibrium model for K^+–Ca^{2+}–Mg^{2+}–NH_4^+–Na^+–SO_4^{2-}–NO_3^-–Cl^-–H_2O aerosols, Atmos. Chem. Phys., 7, 4639–4659, doi:10.5194/acp-7-4639-2007, 2007.

Giorgi, F. and Chameides, W. L.: Rainout lifetimes of highly soluble aerosols and gases as inferred from simulations with a general circulation model, J. Geophys. Res.-Atmos., 91, 14367–14376, 1986.

Gong, S.: A parameterization of sea-salt aerosol source function for sub-and super-micron particles, Global Biogeochem. Cy., 17, 1097, doi:10.1029/2003GB002079, 2003.

Hauglustaine, D. A., Balkanski, Y., and Schulz, M.: A global model simulation of present and future nitrate aerosols and their direct radiative forcing of climate, Atmos. Chem. Phys., 14, 11031–11063, doi:10.5194/acp-14-11031-2014, 2014.

Heald, C. L., Henze, D. K., Horowitz, L. W., Feddema, J., Lamarque, J.-F., Guenther, A., Hess, P. G., Vitt, F., Seinfeld, J. H., Goldstein, A. H. and Fung, I.: Predicted change in global secondary organic aerosol concentrations in response to future climate, emissions, and land use change, J. Geophys. Res., 113, D05211, doi:10.1029/2007JD009092, 2008.

Jaeglé, L., Quinn, P. K., Bates, T. S., Alexander, B., and Lin, J.-T.: Global distribution of sea salt aerosols: new constraints from in situ and remote sensing observations, Atmos. Chem. Phys., 11, 3137–3157, doi:10.5194/acp-11-3137-2011, 2011.

Joly, M. and Peuch, V.-H.: Objective classification of air quality monitoring sites over Europe, Atmos. Environ., 47, 111–123, 2012.

Köpke, P., Hess, M., Schult, I., and Shettle, E.: Global Aerosol Data Set, Max-Planck-Institut für Meteorologie, Hamburg, Germany, 1997.

Koren, I., Remer, L. A., Kaufman, Y. J., Rudich, Y., and Martins, J. V.: On the twilight zone between clouds and aerosols, Geophys. Res. Lett., 34, L08805, doi:10.1029/2007GL029253, 2007.

Kuenen, J. J. P., Visschedijk, A. J. H., Jozwicka, M., and Denier van der Gon, H. A. C.: TNO-MACC_II emission inventory; a multi-year (2003–2009) consistent high-resolution European emission inventory for air quality modelling, Atmos. Chem. Phys., 14, 10963–10976, doi:10.5194/acp-14-10963-2014, 2014.

Lacressonnière, G.: Etude par modélisation numérique de la qualité de l'air en Europe dans les climats actuel et futur, PhD thesis, Université Toulouse III – Paul Sabatier, Centre National de Recherches Météorologiques/Groupe d'étude de l'Atmosphère Météorologique, CNRS-Météo-France, Toulouse, France, 2012.

Lacressonnière, G., Peuch, V.-H., Arteta, J., Josse, B., Joly, M., Marécal, V., Saint Martin, D., Déqué, M., and Watson, L.: How realistic are air quality hindcasts driven by forcings from climate model simulations?, Geosci. Model Dev., 5, 1565–1587, doi:10.5194/gmd-5-1565-2012, 2012.

Lamarque, J.-F., Bond, T. C., Eyring, V., Granier, C., Heil, A., Klimont, Z., Lee, D., Liousse, C., Mieville, A., Owen, B., Schultz, M. G., Shindell, D., Smith, S. J., Stehfest, E., Van Aardenne, J., Cooper, O. R., Kainuma, M., Mahowald, N., McConnell, J. R., Naik, V., Riahi, K., and van Vuuren, D. P.: Historical (1850–2000) gridded anthropogenic and biomass burning emissions of reactive gases and aerosols: methodology and application, Atmos. Chem. Phys., 10, 7017–7039, doi:10.5194/acp-10-7017-2010, 2010.

Lamarque, J.-F., Shindell, D. T., Josse, B., Young, P. J., Cionni, I., Eyring, V., Bergmann, D., Cameron-Smith, P., Collins, W. J., Doherty, R., Dalsoren, S., Faluvegi, G., Folberth, G., Ghan, S. J., Horowitz, L. W., Lee, Y. H., MacKenzie, I. A., Nagashima, T., Naik, V., Plummer, D., Righi, M., Rumbold, S. T., Schulz, M., Skeie, R. B., Stevenson, D. S., Strode, S., Sudo, K., Szopa, S., Voulgarakis, A., and Zeng, G.: The Atmospheric Chemistry and Climate Model Intercomparison Project (ACCMIP): overview and description of models, simulations and climate diagnostics, Geosci. Model Dev., 6, 179–206, doi:10.5194/gmd-6-179-2013, 2013.

Lefèvre, F., Brasseur, G., Folkins, I., Smith, A., and Simon, P.: Chemistry of the 1991–1992 stratospheric winter: three-dimensional model simulations, J. Geophys. Res.-Atmos., 99, 8183–8195, 1994.

Liu, H., Jacob, D. J., Bey, I., and Yantosca, R. M.: Constraints from 210Pb and 7Be on wet deposition and transport in a global three-dimensional chemical tracer model driven by assimilated meteorological fields, J. Geophys. Res.-Atmos., 106, 12109–12128, 2001.

Louis, J.-F.: A parametric model of vertical eddy fluxes in the atmosphere, Bound.-Lay. Meteorol., 17, 187–202, 1979.

Marécal, V., Peuch, V.-H., Andersson, C., Andersson, S., Arteta, J., Beekmann, M., Benedictow, A., Bergström, R., Bessagnet, B., Cansado, A., Chéroux, F., Colette, A., Coman, A., Curier, R. L., Denier van der Gon, H. A. C., Drouin, A., Elbern, H., Emili, E., Engelen, R. J., Eskes, H. J., Foret, G., Friese, E., Gauss, M., Giannaros, C., Guth, J., Joly, M., Jaumouillé, E., Josse, B., Kadygrov, N., Kaiser, J. W., Krajsek, K., Kuenen, J., Kumar, U., Liora, N., Lopez, E., Malherbe, L., Martinez, I., Melas, D., Meleux, F., Menut, L., Moinat, P., Morales, T., Parmentier, J., Piacentini, A., Plu, M.,

Poupkou, A., Queguiner, S., Robertson, L., Rouïl, L., Schaap, M., Segers, A., Sofiev, M., Thomas, M., Timmermans, R., Valdebenito, Á., van Velthoven, P., van Versendaal, R., Vira, J., and Ung, A.: A regional air quality forecasting system over Europe: the MACC-II daily ensemble production, Geosci. Model Dev. Discuss., 8, 2739–2806, doi:10.5194/gmdd-8-2739-2015, 2015.

Mari, C., Jacob, D. J., and Bechtold, P.: Transport and scavenging of soluble gases in a deep convective cloud, J. Geophys. Res.-Atmos., 105, 22255–22267, 2000.

Martet, M., Peuch, V., Laurent, B., Marticorena, B., and Bergametti, G.: Evaluation of long-range transport and deposition of desert dust with the CTM MOCAGE, Tellus B, 61, 449–463, 2009.

Marticorena, B. and Bergametti, G.: Modeling the atmospheric dust cycle: 1. Design of a soil-derived dust emission scheme, J. Geophys. Res.-Atmos., 100, 16415–16430, 1995.

Ménégoz, M., Salas y Melia, D., Legrand, M., Teyssèdre, H., Michou, M., Peuch, V.-H., Martet, M., Josse, B., and Dombrowski-Etchevers, I.: Equilibrium of sinks and sources of sulphate over Europe: comparison between a six-year simulation and EMEP observations, Atmos. Chem. Phys., 9, 4505–4519, doi:10.5194/acp-9-4505-2009, 2009.

Nenes, A., Pandis, S., and Pilinis, C.: ISORROPIA: a new thermodynamic equilibrium model for multiphase multicomponent inorganic aerosols, Aquat. Geochem., 4, 123–152, doi:10.1023/A:1009604003981, 1998.

Olivier, J., Bouwman, A., Van der Hoek, K., and Berdowski, J.: Global air emission inventories for anthropogenic sources of NO_x, NH_3 and N_2O in 1990, Environ. Pollut., 102, 135–148, 1998.

Paulot, F., Jacob, D. J., Johnson, M. T., Bell, T. G., Baker, A. R., Keene, W. C., Lima, I. D., Doney, S. C., and Stock, C. A.: Global oceanic emission of ammonia: Constraints from seawater and atmospheric observations, Global Biogeochem. Cycles, 29, 1165–1178, doi:10.1002/2015GB005106, 2015.

Pham, M., Müller, J.-F., Brasseur, G., Granier, C., and Megie, G.: A three-dimensional study of the tropospheric sulfur cycle, J. Geophys. Res., 100, 26061–26092, 1995.

Price, C., Penner, J., and Prather, M.: NO_x from lightning: 1. Global distribution based on lightning physics, J. Geophys. Res.-Atmos., 102, 5929–5941, doi:10.1029/96JD03504, 1997.

Querol, X., Alastuey, A., Ruiz, C., Artinano, B., Hansson, H., Harrison, R., Buringh, E. T., Ten Brink, H., Lutz, M., Bruckmann, P., Straehl, P., and Schneider, J.: Speciation and origin of PM_{10} and $PM_{2.5}$ in selected European cities, Atmos. Environ., 38, 6547–6555, 2004.

Remer, L. A., Kleidman, R. G., Levy, R. C., Kaufman, Y. J., Tanré, D., Mattoo, S., Martins, J. V., Ichoku, C., Koren, I., Yu, H., and Holben, B. N.: Global aerosol climatology from the MODIS satellite sensors, J. Geophys. Res.-Atmos., 113, D14S07, doi:10.1029/2007JD009661, 2008.

Rouil, L., Honoré, C., Bessagnet, B., Malherbe, L., Meleux, F., Vautard, R., Beekmann, M., Flaud, J.-M., Dufour, A., Martin, D., Peuch, A., Peuch, V.-H., Elichegaray, C., Poisson, N., and Menut, L.: PREV'AIR: an operational forecasting and mapping system for air quality in Europe, B. Am. Meteorol. Soc., 90, 73–83, 2009.

Ruiz-Arias, J. A., Dudhia, J., Gueymard, C. A., and Pozo-Vázquez, D.: Assessment of the Level-3 MODIS daily aerosol optical depth in the context of surface solar radiation and numerical weather modeling, Atmos. Chem. Phys., 13, 675–692, doi:10.5194/acp-13-675-2013, 2013.

Saiz-Lopez, A. and von Glasow, R.: Reactive halogen chemistry in the troposphere, Chem. Soc. Rev., 41, 6448–6472, doi:10.1039/C2CS35208G, 2012.

Schaap, M., van Loon, M., ten Brink, H. M., Dentener, F. J., and Builtjes, P. J. H.: Secondary inorganic aerosol simulations for Europe with special attention to nitrate, Atmos. Chem. Phys., 4, 857–874, doi:10.5194/acp-4-857-2004, 2004.

Schaap, M., Timmermans, R. M., Roemer, M., Boersen, G., Builtjes, P., Sauter, F., Velders, G., and Beck, J.: The LOTOS-EUROS model: description, validation and latest developments, Int. J. Environ. Pollut., 32, 270–290, 2008.

Seigneur, C., Pun, B., Pai, P., Louis, J.-F., Solomon, P., Emery, C., Morris, R., Zahniser, M., Worsnop, D., Koutrakis, P., White, W., and Tombach, I.: Guidance for the performance evaluation of three-dimensional air quality modeling systems for particulate matter and visibility, JAPCA J. Air Waste Ma., 50, 588–599, doi:10.1080/10473289.2000.10464036, 2000.

Seinfeld, J. and Pandis, S.: Atmospheric Chemistry and Physics, John Wiley, Hoboken, NJ, 1326 pp., 1998.

Sič, B., El Amraoui, L., Marécal, V., Josse, B., Arteta, J., Guth, J., Joly, M., and Hamer, P. D.: Modelling of primary aerosols in the chemical transport model MOCAGE: development and evaluation of aerosol physical parameterizations, Geosci. Model Dev., 8, 381–408, doi:10.5194/gmd-8-381-2015, 2015.

Sindelarova, K., Granier, C., Bouarar, I., Guenther, A., Tilmes, S., Stavrakou, T., Müller, J.-F., Kuhn, U., Stefani, P., and Knorr, W.: Global data set of biogenic VOC emissions calculated by the MEGAN model over the last 30 years, Atmos. Chem. Phys., 14, 9317-9341, 10.5194/acp-14-9317-2014, 2014.

Slinn, W.: Some approximations for the wet and dry removal of particles and gases from the atmosphere, Water Air Soil Poll., 7, 513–543, 1977.

Slinn, W.: Estimates for the long-range transport of air pollution, in: Long-Range Transport of Airborne Pollutants, Springer, 45–64, 1982.

Stocker, T. F., Qin, D., Plattner, G.-K., Tignor, M., Allen, S. K., Boschung, J., Nauels, A., Xia, Y., Bex, V., and Midgley, P. M.: Climate Change 2013: the Physical Science Basis, Intergovernmental

Panel on Climate Change, Working Group I Contribution to the IPCC Fifth Assessment Report (AR5), Cambridge Univ Press, New York, 2013.
Stockwell, W., Kirchner, F., Kuhn, M., and Seefeld, S.: A new mechanism for regional atmospheric chemistry modeling, J. Geophys. Res., 102, 25847–25879, 1997.
Teyssèdre, H., Michou, M., Clark, H. L., Josse, B., Karcher, F., Olivié, D., Peuch, V.-H., Saint-Martin, D., Cariolle, D., Attié, J.-L., Nédélec, P., Ricaud, P., Thouret, V., van der A, R. J., Volz-Thomas, A., and Chéroux, F.: A new tropospheric and stratospheric Chemistry and Transport Model MOCAGE-Climat for multi-year studies: evaluation of the present-day climatology and sensitivity to surface processes, Atmos. Chem. Phys., 7, 5815–5860, doi:10.5194/acp-7-5815-2007, 2007.
Tsigaridis, K. and Kanakidou, M.: Global modelling of secondary organic aerosol in the troposphere: a sensitivity analysis, Atmos. Chem. Phys., 3, 1849-1869, doi:10.5194/acp-3-1849-2003, 2003.
Tørseth, K., Aas, W., Breivik, K., Fjæraa, A. M., Fiebig, M., Hjellbrekke, A. G., Lund Myhre, C., Solberg, S., and Yttri, K. E.: Introduction to the European Monitoring and Evaluation Programme (EMEP) and observed atmospheric composition change during 1972–2009, Atmos. Chem. Phys., 12, 5447–5481, doi:10.5194/acp-12-5447-2012, 2012.
Vogel, B., Vogel, H., Bäumer, D., Bangert, M., Lundgren, K., Rinke, R., and Stanelle, T.: The comprehensive model system COSMO-ART – Radiative impact of aerosol on the state of the atmosphere on the regional scale, Atmos. Chem. Phys., 9, 8661–8680, doi:10.5194/acp-9-8661-2009, 2009.
Wesely, M.: Parameterization of surface resistances to gaseous dry deposition in regional-scale numerical models, Atmos. Environ., 23, 1293–1304, 1989.
Wexler, A. S. and Seinfeld, J. H.: The distribution of ammonium salts among a size and composition dispersed aerosol, Atmos. Environ. A-Gen., 24, 1231–1246, 1990.
WHO: WHO Air quality guidelines for particulate matter, ozone, nitrogen dioxide and sulfur dioxide: global update 2005: summary of risk assessment, World Health Organization, 2006.
Williamson, D. L. and Rasch, P. J.: Two-dimensional semi-Lagrangian transport with shape-preserving interpolation, Mon. Weather Rev., 117, 102–129, 1989.
Wiscombe, W. J.: Improved Mie scattering algorithms, Appl. Optics, 19, 1505–1509, 1980.
Xu, L. and Penner, J. E.: Global simulations of nitrate and ammonium aerosols and their radiative effects, Atmos. Chem. Phys., 12, 9479–9504, doi:10.5194/acp-12-9479-2012, 2012.
Zhang, J., Reid, J. S., and Holben, B. N.: An analysis of potential cloud artifacts in MODIS over ocean aerosol optical thickness products, Geophys. Res. Lett., 32, L15803, doi:10.1029/2005GL023254, 2005.

Zhuang, H., Chan, C. K., Fang, M., and Wexler, A. S.: Size distributions of particulate sulfate, nitrate, and ammonium at a coastal site in Hong Kong, Atmos. Environ., 33, 843–853, 1999.

Table 1. Summary of the heterogeneous formation processes of secondary inorganic aerosols precursors that have been in the model. $k_1 = 7.5 \times 10^7 e^{-4430\left(\frac{1}{T}-\frac{1}{298}\right)}$, T is the ambiant temperature, P the pressure, $k_2 = 2.4 \times 10^4$, $k_3 = 3.7 \times 10^5 . e^{-5530\left(\frac{1}{T}-\frac{1}{298}\right)}$ and $k_4 = 1.5 \times 10^9 . e^{-5280\left(\frac{1}{T}-\frac{1}{298}\right)}$. D_g ($\mathrm{cm^2 s^{-1}}$) is the gas phase diffusion coefficient, r the aerosol radius, v the mean molecular speed ($\mathrm{cm\,s^{-1}}$), and γ the reaction probability being 0.1.

Compound	Formation reaction	Reaction rate
H_2SO_4	Aqueous phase oxydation	$\mathrm{H_2O_2} : \frac{dS}{dt} = \frac{k_1 \left[\mathrm{H^+}\right] \left[\mathrm{H_2O_2}\right] \left[\mathrm{HSO_3^-}\right]}{1+P\left[\mathrm{H^+}\right]}$ $\mathrm{O_3} : \frac{dS}{dt} = \left(k_2 \left[\mathrm{SO_{2}}_{aq}\right] + k_3 \left[HSO^-\right] + k_4 \left[SO_3^{2-}\right]\right) \left[\mathrm{O_3}\right]$
HNO_3	N_2O_5 hydrolysis	$\left(\frac{r}{G_g} + \frac{4}{v\gamma}\right)^{-1} A$
NH_3	Only emitted	–

Table 2. List of the liquid aerosol species given by ISORROPIA model.

Liquid aerosol species
H^+
NA^+
NH_4^+
Cl^-
SO_4^{2-}
HSO_4^-
NO_3^-
H_2O
NH_3
HCl
HNO_3
OH^-

Table 3. List of the solid aerosol species given by ISORROPIA model.

Solid aerosol species
$NaNO_3$
NH_4NO_3
$NaCl$
Na_2SO_4
$NaHSO_4$
$(NH_4)_2SO_4$
$NAHSO_4$
NH_4HSO_4
$(NH_4)_4H(SO_4)_2$

Table 4. List of the gaseous compounds given by ISORROPIA model.

Gaseous compounds
HCl
HNO_3
NH_3

Table 5. Mass mean aerodynamic diameter of the distribution modes from Zhuang et al. (1999).

mode in μm	Sulfates	Ammoniums	Nitrates
Condensation mode	0.2 ± 0.15	0.21 ± 0.10	0.14 ± 0.22
Droplet mode	0.58 ± 0.11	0.56 ± 0.10	0.46 ± 0.33
Coarse mode	4.2 ± 2	5.7 ± 2	3.95 ± 0.69

Table 6. Secondary inorganic aerosol compound statistics of RACMSIA simulation daily HTAP observations.

Compound	number of stations	number of observations	MNMB	FGE	Correlation
Sulfate total	94	30 754	0.05	0.94	0.33
Sulfate corrected	21	7098	−0.12	0.73	0.70
Nitrate	61	19 410	−0.13	0.94	0.53
Ammonium	51	15 765	0.19	0.74	0.69

Table 7. Statistics of daily observation at the same Irish as in Fig. 7 against RACMSIA simulation.The parameter sulfate corresponds to corrected sulfate.

Compound	MNMB	FGE	Correlation
Sulfate	−0.19	0.53	0.65
Nitrate	0.17	0.54	0.77
Ammonium	0.02	0.46	0.71

1

Table 8. Statistics of daily observation at the canadian station (CA0008R) located east of Lake Superios against RACMSIA simulation. The parameter sulfate corresponds to total sulfate and the modelled field takes into account a part of sulfate in sea salt.

Compound	MNMB	FGE	Correlation
Sulfate	−0.41	0.85	0.50
Nitrate	−0.60	1.24	0.16
Ammonium	−0.29	0.86	0.56

Table 9. Gaseous compounds statistics of simulation results against daily HTAP observations. Comparison between a simulation with SIA (RACMSIA) and without SIA formation (RACM).

			MNMB		FGE		Correlation	
Compound	number of stations	number of observations	RACM	RACMSIA	RACM	RACMSIA	RACM	RACMSIA
Sulfur dioxide	69	23 325	1.21	1.21	1.37	1.37	0.53	0.53
Nitrogen dioxide	41	14 122	0.61	0.53	0.83	0.77	0.55	0.57
Nitric acid	30	10 033	0.45	−0.13	0.88	0.99	0.46	0.33
Ammonia	20	6381	1.84	0.79	1.84	1.27	0.18	0.33

Table 10. Secondary inorganic aerosol compounds statistics of RACMSIA simulation against weekly HTAP observations.

Compound	number of stations	number of observations	MNMB	FGE	Correlation
Sulfate total	192	19 203	−0.05	0.67	0.64
Sulfate corrected	1	52	−0.12	0.63	0.51
Nitrate	190	19 066	0.06	1.00	0.41
Ammonium	43	1595	0.34	0.84	0.43

Table 11. Secondary inorganic aerosol compounds statistics of RACMSIA simulation against weekly HTAP observations, separation between North America (N. A.) and Asia.

	Stations		MNMB		FGE		Correlation	
Compound	N. A.	Asia	N. A.	Asia	N. A.	Asia	N. A.	Asia
Sulfate total	161	28	−0.03	−0.05	0.67	0.68	0.65	0.64
Nitrate	161	28	0.05	0.30	0.99	1.16	0.41	0.13
Ammonium	14	28	0.27	0.35	0.60	0.96	0.19	0.41

Table 12. Secondary inorganic aerosols statistics of RACMSIA simulation against daily EMEP observations.

Compound	number of stations	number of observations	MNMB	FGE	Correlation
Sulfate total	66	19 861	−0.16	0.67	0.57
Sulfate corrected	34	9705	−0.33	0.73	0.68
Nitrate	49	13 360	−0.08	0.87	0.53
Ammonium	40	10 406	0.18	0.69	0.71

Table 13. Gaseous compounds statistics of simulation results against daily EMEP observations. Comparison between a simulation with SIA (RACMSIA) and without SIA formation (RACM).

			MNMB		FGE		Correlation	
Compound	number of stations	number of observations	RACM	RACMSIA	RACM	RACMSIA	RACM	RACMSIA
Sulfur dioxide	47	14861	0.97	0.98	1.15	1.15	0.60	0.60
Nitrogen dioxide	44	14809	0.18	0.10	0.74	0.69	0.57	0.59
Nitric acid	12	3290	0.55	−0.15	0.99	1.08	0.36	0.26
Ammonia	40	5324	1.61	0.46	1.62	1.18	−0.01	0.24

Table 14. Air quality regulated pollutants statistics of simulations against hourly AIRBASE observations. Comparison between a simulation with SIA (RACMSIA) and without SIA formation (RACM).

		MNMB		FGE		Correlation	
Compound	number of Stations	RACM	RACMSIA	RACM	RACMSIA	RACM	RACMSIA
$PM_{2.5}$	1082	−0.58	−0.14	0.77	0.56	0.47	0.58
PM_{10}	1082	−0.89	−0.45	0.97	0.66	0.39	0.50
O_3	1168	0.31	0.27	0.42	0.41	0.63	0.60
NO_2	610	−0.10	−0.13	0.66	0.65	0.54	0.53

Table 15. Comparison of MNMB statistics between MOCAGE simulations (RACM and RACMSIA) and AIRBASE data over Europe for $PM_{2.5}$ according to different seasons.

$PM_{2.5}$ MNMB	RACM	RACMSIA	Δ
Year	-0.58	-0.14	$+0.44$
MAM	-0.55	-0.03	$+0.52$
JJA	-0.62	-0.27	$+0.35$
SON	-0.44	-0.07	$+0.37$

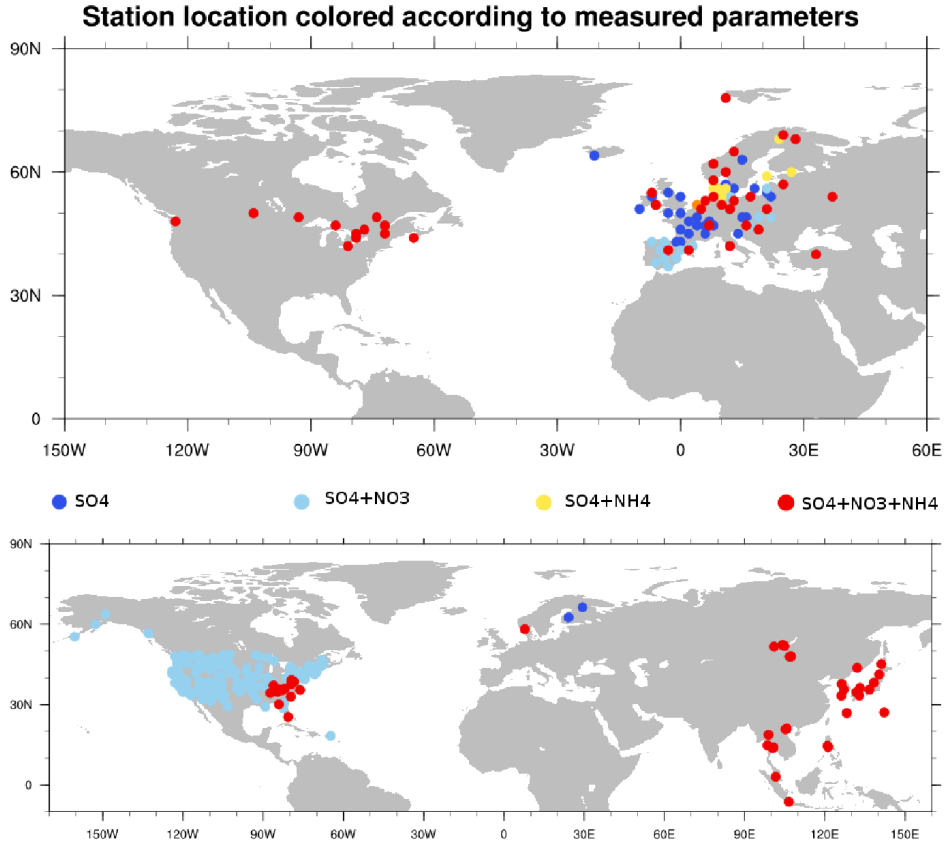

Figure 1. Maps with the location of the stations measuring in 2005 used to evaluate the model. Colors represent the measured parameters at the station. The upper panel represents daily observation stations while the bottom panel represents weekly observation stations.

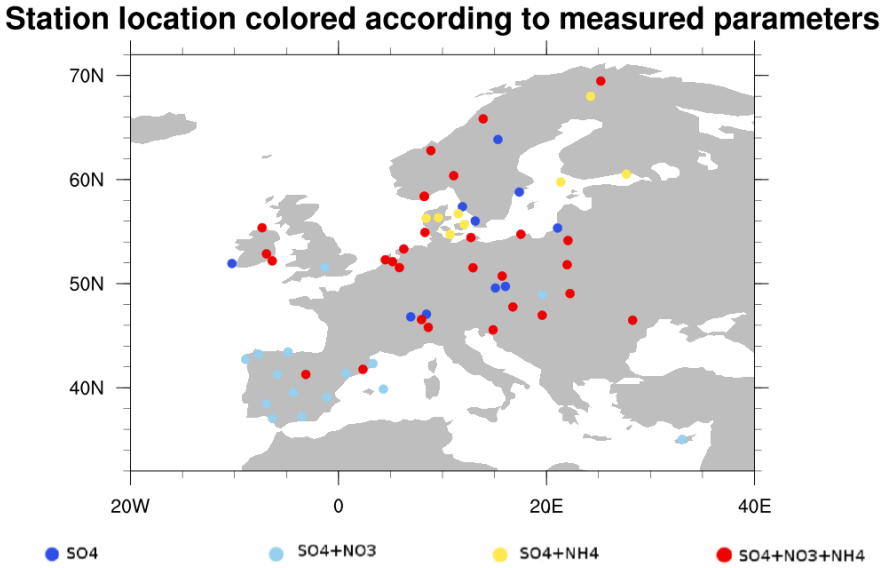

Figure 2. Map with the location of the stations measuring SIA composition on a daily basis, from the EMEP database used to evaluate the regional model results. Colors represent the measured parameters at the station. The domain plotted corresponds to the limit of the regional domain of the simulation. Colors represent the altitude of the stations.

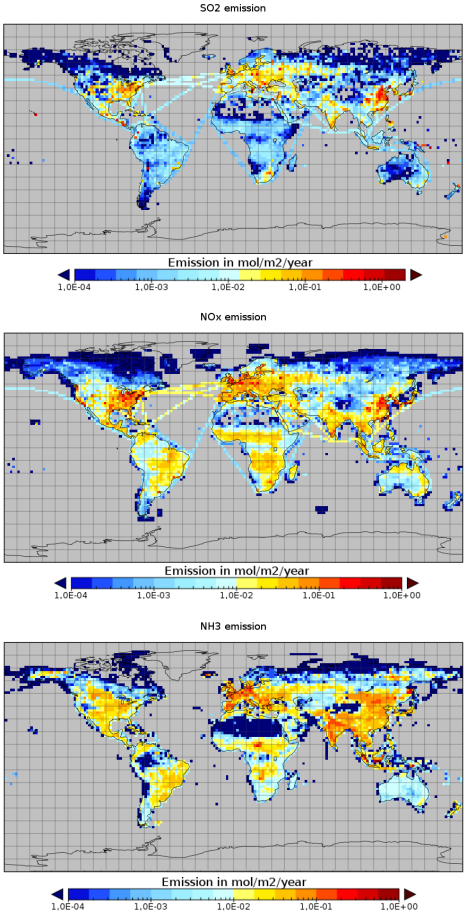

Figure 3. Maps of 2005 annual emissions of sulfur dioxide (SO_2) (top panel), nitrous oxides (NO_x) (middle panel) and ammonia (NH_3) (bottom panel), in $\mathrm{mol\,m^{-2}\,year^{-1}}$ for the MOCAGE simulations (RACM and RACMSIA).

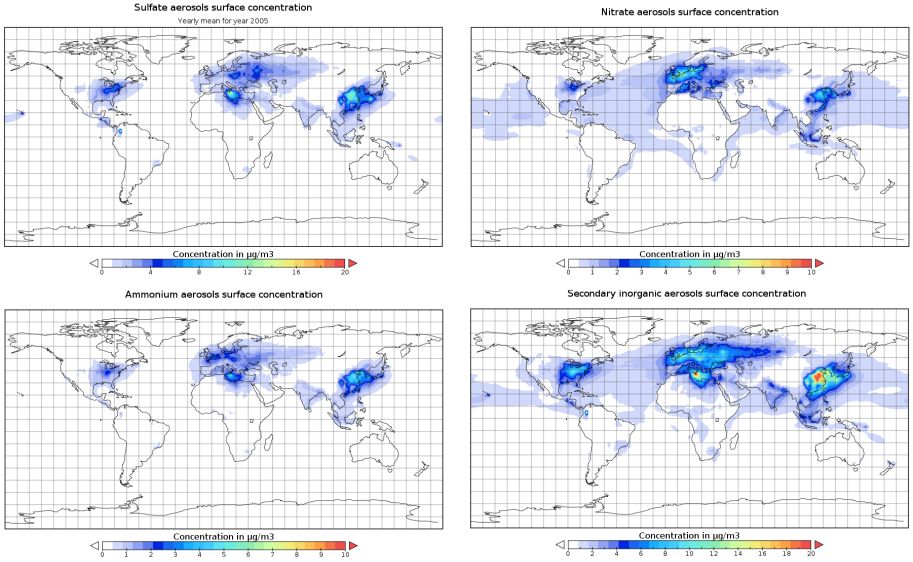

Figure 4. Maps of global annual mean concentrations at the surface, in $\mu g\,m^{-3}$ of secondary inorganic aerosols components from the RACMSIA simulation. Top left panel is sulfate, top right panel nitrate, bottom left panel ammonium and bottom right panel is the sum of the three components.

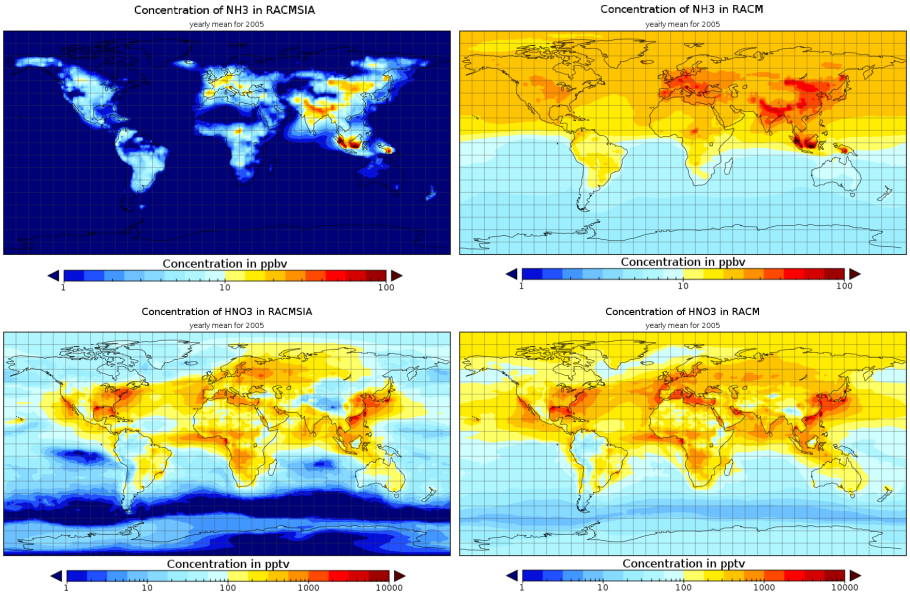

Figure 5. Maps of global annual mean concentrations of NH_3 in ppbv (top panels) and HNO_3 in pptv (bottom panels) for both simulations RACMSIA (left side) and RACM (right side).

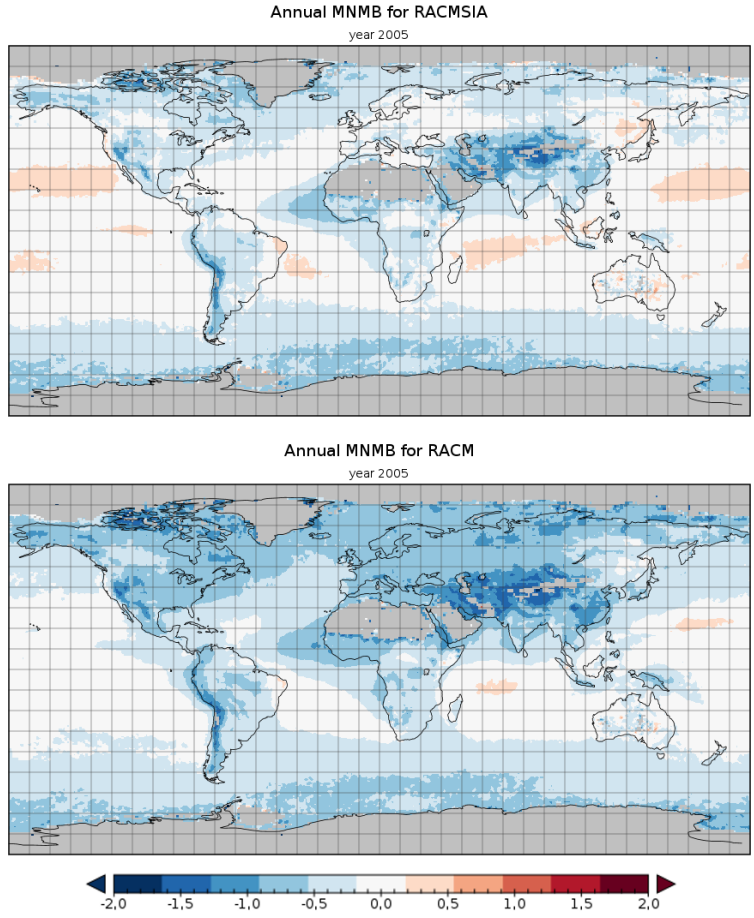

Figure 6. Maps of annual modified normalised mean bias (MNMB) of aerosol optical depth against MODIS observations. The upper panel shows the RACM experiment while the lower panel the RACM-SIA experiment with secondary inorganic aerosols.

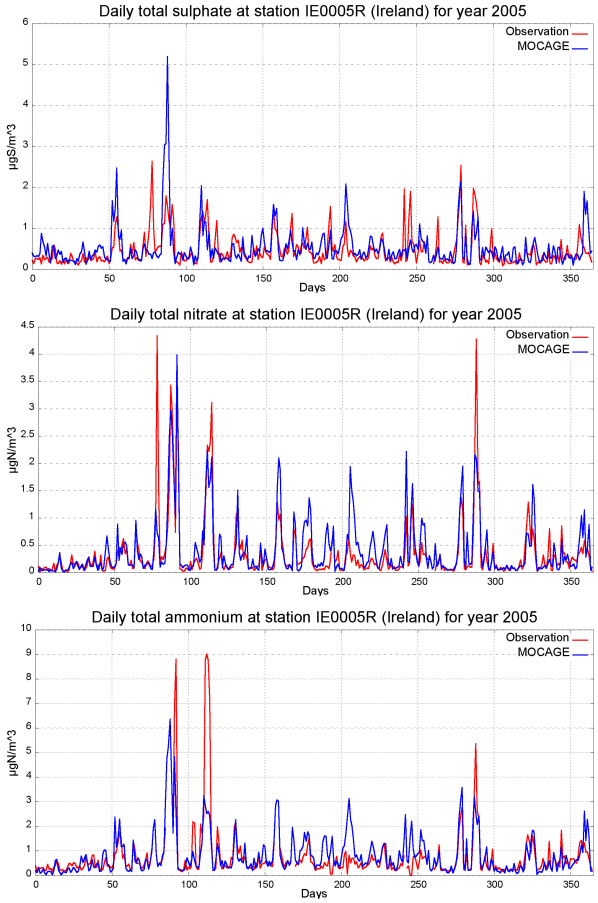

Figure 7. Time-series of daily values (in $\mu g\,m^{-3}$) of sulfate (top panel), nitrate (middle panel) and ammonium (bottom panel) at an Irish station ($52.87°$ N; $6.92°$ W) against RACMSIA simulation for the year 2005.

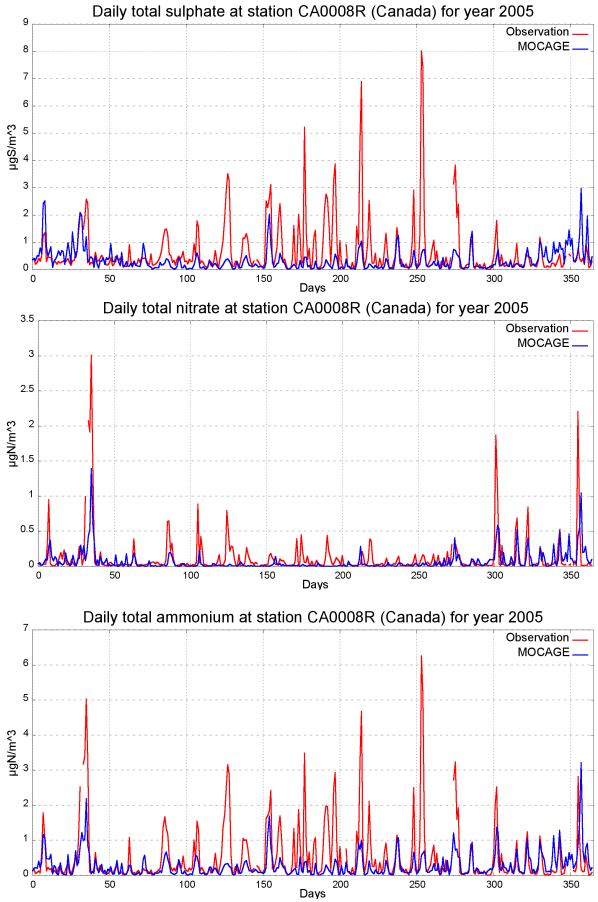

Figure 8. Time-series of daily values (in $\mu g\,m^{-3}$) of sulfate (top panel), nitrate (middle panel) and ammonium (bottom panel) at a Canadian station ($47.03°$ N; $-84.38°$ W) against RACMSIA simulation for the year 2005.

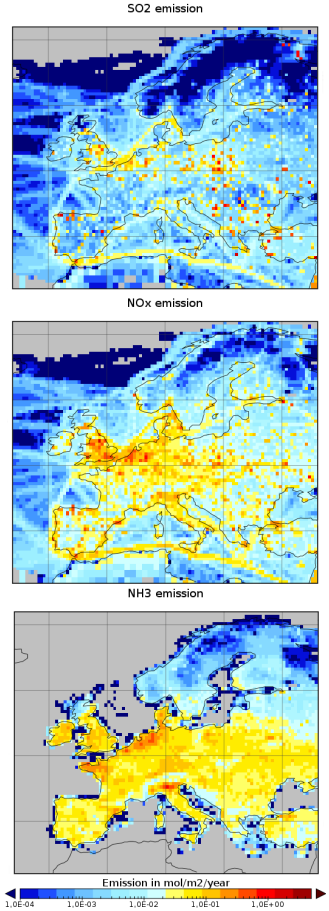

Figure 9. Maps of annual emissions for sulfur dioxide (top panel), nitrous oxides (middle panel) and ammonia (bottom panel) in $\mathrm{mol\,m^{-2}\,year^{-1}}$ for the MOCAGE simulations (RACM and RACMSIA).

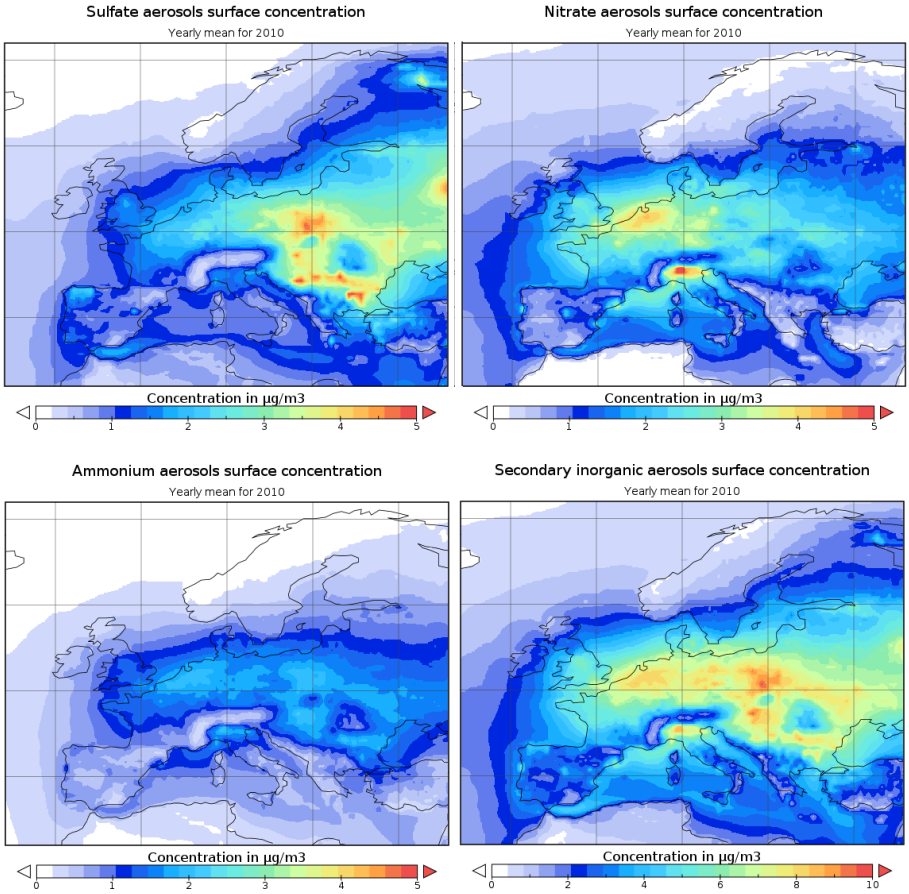

Figure 10. Maps of regional annual mean concentrations, in $\mu g\,m^{-3}$ of secondary inorganic aerosols components over a regional domain for the year 2010 for the RACMSIA simulation. Top left panel represents sulfate concentration, top right nitrate, bottom left ammonium and bottom right represents the sum of these three SIA components.

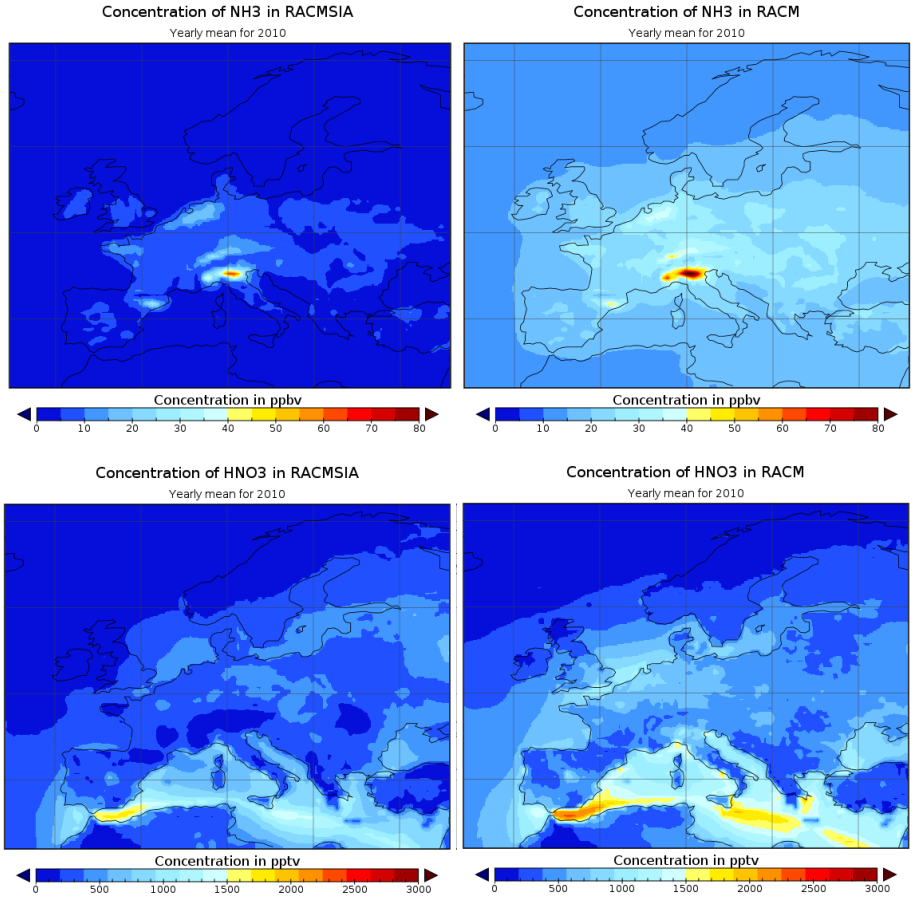

Figure 11. Maps of regional annual mean concentrations of NH_3 in ppbv (top panels) and HNO_3 in pptv (bottom panels) for both simulations RACMSIA (left side) and RACM (right side).

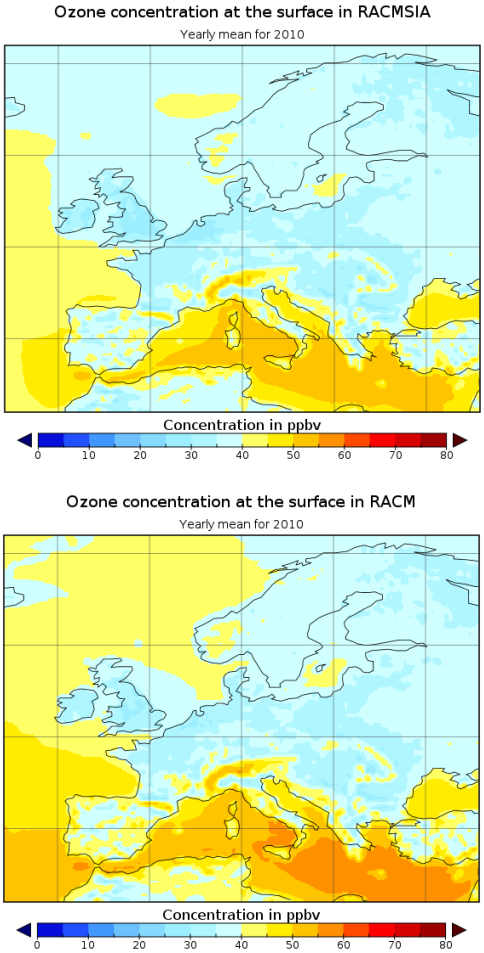

Figure 12. Maps of regional annual mean ozone concentrations for the year 2010 in ppbv. Top panel represents RACMSIA simulation and bottom panel the RACM simulation.